Received: 27 May 2025 | Revised: 19 September 2025 | Accepted: 31 October 2025

DOI: 10.1002/qj.70075

Quarterly Journal of the Royal Meteorological Society RMetS

RESEARCH ARTICLE

Assessing wildfire dynamics during a megafire in Portugal using the MesoNH/ForeFire coupled model

Cátia Campos[1] | **Flavio Tiago Couto**[1,2] | **Filippe L. M. Santos**[1] | **Paulo Pinto**[3] | **Carolina Purificação**[1,3] | **Hugo Miguel Silva**[4] | **João Rio**[1,3] | **Manuel Lopes**[3] | **Roberta Baggio**[5] | **Jean-Baptiste Filippi**[5] | **Maria José Monteiro**[3] | **Daniele Bortoli**[1,2] | **Rui Salgado**[1,2]

[1]Centro de Investigação em Ciência e Tecnologia Para o Sistema Terra e Energia — CREATE, Universidade de Évora, Évora, Portugal

[2]Departamento de Física, Escola de Ciências e Tecnologia, Universidade de Évora, Évora, Portugal

[3]Portuguese Institute for Sea and Atmosphere, I.P., Rua C do Aeroporto, Lisbon, Portugal

[4]Coleção de Insetos da Universidade da Madeira, Faculdade de Ciências da Vida, Campus Universitário da Penteada, Universidade da Madeira, Funchal, Portugal

[5]Centre National de la Recherche Scientifique (CNRS), Sciences Pour l'Environnement, Università di Corsica, Corte, France

Correspondence
Cátia Campos, Centro de Investigação em Ciência e Tecnologia Para o Sistema Terra e Energia – CREATE, Universidade de Évora, Rua Romão Ramalho, 59, Évora, Portugal.
Email: catia.campos@uevora.pt

Funding information
Fundação para a Ciência e a Tecnologia, Grant/Award Numbers: 2022.11960.BD, 2024.05649.BD, PCIF/MPG/0175/2019, UIDB/06107; European Commission, Grant/Award Number: 0139_FIREPOCTEP_MAS_6_E

Abstract

This study investigates the Serra da Estrela megafire, located in Portugal, which occurred in August 2022, aiming to explore how changes in weather conditions can modify fire behavior in a fire burning during several days. The study uses a set of fire–atmosphere coupled simulations, referred as EXPn. The MesoNH atmospheric model was coupled to the ForeFire fire propagation model and configured with three nested domains, each comprising a 150 × 150 horizontal grid, with resolutions of 1500 m, 500 m, and 250 m. Regarding the experiments, EXP1 [IGN] corresponds to the ignition phase on 6 August, EXP2 [PYRO] to the development of pyro-convective clouds on 10 August, whereas EXP3 [REAC] represents the fire reactivation period on 15 August. The first and third periods showed that smoke plumes were transported mainly within the boundary layer, whereas in the second period pyro-convection reached the middle tropospheric levels, allowing the formation of pyro-convective clouds. Such clouds were confirmed from radar and satellite observations. Beside the fire-generated clouds, the study highlighted that propagation of the fire front can suddenly shift due to the interaction between weather, fire and complex terrain. This study confirmed the importance of the use of coupled atmosphere–fire models to represent fire dynamics and their impact on local meteorology. In a global perspective, such an approach provides a framework for assessing wildfire–atmosphere interactions in diverse environments, supporting improved prediction of large wildfires. Overall, it underscores the influence of evolving atmospheric conditions on fire behavior, which is critical for understanding the development of megafires capable of burning over several weeks. This study highlights the crucial need to expand our scientific understanding of fire behavior, enabling its application to other regions worldwide.

KEYWORDS

fire meteorology, megafire, MesoNH/ForeFire, pyro-convective clouds

1 | INTRODUCTION

Wildfires result from several chemical and physical processes and interactions across different temporal and spatial scales. These complex interactions range from the combustion and release of energy from vegetative fuels and the transfer of heat to adjacent fuels to interactions with regional or large-scale atmospheric flow (Sullivan, 2017). Fire behavior, in turn, can be summarized by the fire triangle consisting of meteorology, fuel, and topography (Countryman, 1972; Güngöroğlu, 2018). These components interact in complex ways that directly influence fire spread, fire intensity, and the fuel flammability.

Given the complexity of wildfire development, considerable efforts have been made to better understand fire–atmosphere interactions, namely through numerical modeling. Several coupled models have been tested to explore these fire–atmosphere processes; notably, MesoNH/ForeFire, WRF-SFIRE, and ACCESS-Fire explicitly account for fire–atmosphere feedbacks and have been applied in case studies worldwide. For instance, both MesoNH/ForeFire and WRF-SFire have been used to investigate major wildfires in Portugal (Campos et al., 2023; Couto et al., 2024a, b; Vaz et al., 2025); in Greece, similar analyses were conducted by Kartsios et al. (2021); in Australia, the ACCESS-Fire system has been applied (Peace et al., 2022, Peace et al., 2023); and in the United States, Clough et al. (2025) and Cheung et al. (2025), have employed WRF-SFIRE to study fire–atmosphere dynamics. Additionally, Toivanen et al. (2019) used the UK Met Office Unified Model coupled with the McArthur fire spread model to simulate a wildfire in Australia.

In recent years, extreme wildfires, commonly known as megafires (exceeding 10,000 hectares; Linley et al., 2022) have been reported around the world. For instance, Australia's 'Black Summer' fire season of 2019–2020 burned around 530,000 hectares (Peterson et al., 2021), pushing several endangered species to the brink of local extinction (Dickman, 2021). In Greece, the 2018 fire season took 102 human lives (Kartsios et al., 2021) while during 2017, Chile had its most severe forest fires on record, with over 500,000 hectares burned (de la Barrera et al., 2018). On the other hand, other regions have reported an increase of wildfires in the last decades, for example, the Indian Himalayan region (Prabhakaran & Srivastava, 2025). According to Almeida et al. (2024), Europe experienced severe weather conditions in 2022 that resulted in more than 800,000 hectares burned. Notably, regions historically less vulnerable to wildfires, such as Slovenia and northeastern Italy, reported significant fire activity. Protected areas also suffered substantially in 2022, with Portugal, Spain, and Romania collectively experiencing over 270,000 hectares of wildfire damage. The 2023 fire season in the Northern Hemisphere brought several catastrophic events. In Greece, a single wildfire consumed 94,000 hectares and caused 28 human fatalities. In Hawaii, wildfires completely destroyed a city, resulting in 100 recorded deaths. In Canada, an unprecedented 15 million hectares burned (Mayers, 2024). These escalating events strongly suggest that climate change has intensified fire potential (Di Virgilio et al., 2019).

The Iberian Peninsula is the European region with the highest wildfire incidence, resulting in significant property damage and fatalities (San-Miguel-Ayanz et al., 2020). Portugal has experienced a long history of wildfires, with severe events in the last decades, particularly in 2003, 2005, and 2017. Inadequate forest and landscape management, demographic shifts, agricultural land abandonment and the expansion of monocultures, namely maritime pine (*Pinus pinaster*) and eucalypt (*Eucalyptus globulus*), have all contributed to increased danger of fire (Bento-Gonçalves, 2021). In the climatic context, the extreme fire seasons primarily resulted from anomalous atmospheric synoptic patterns and extreme fire-weather conditions (Gouveia et al., 2012; Trigo et al., 2006; Turco et al., 2019). Carmo et al. (2021) studied the climatology of extreme fire seasons in mainland Portugal and highlighted that northeasterly and easterly flows are the most dangerous fire-weather conditions. Additional studies have shown that large wildfires are closely correlated with heatwaves and droughts in western Iberia (e.g., Rodrigues et al., 2020). Climate change is projected to impact fire weather in Portugal, with fire activity expected to increase throughout the year, resulting in longer and more severe fire seasons (Calheiros et al., 2021). Early evidence of this trend was documented by Couto et al. (2022) in their study of a 10-year period of winter fires' activity in Portugal. The authors highlighted the record number of fires during winter 2021/2022, which was characterized by unusually mild winter conditions.

Extreme wildfire events are characterized by high intensity and significant energy release. They pose exceptional management challenges and frequently exceed control capacities, resulting in tens of thousands of hectares burned, severe damage to natural heritage and wildlife, and human fatalities. In such cases, the energy released can be so intense that the fire effectively creates its own weather, triggering fire–atmosphere interactions that enable the formation of pyro-convective clouds or/and fire-generated tornadoes (Fromm et al., 2010; Lareau et al., 2018; Lareau & Clements, 2017). These phenomena can influence fire behavior, affecting the rate of spread (ROS) and altering fire front directions (Peterson et al., 2018). Beside fire–atmosphere interaction phenomena influencing ROS, the establishment of

megafires can also be associated with different factors supporting progressive expansion of the burned area. Changes in atmospheric conditions on a subdaily scale can lead to unexpected fire behavior and consequently a sudden increase in the burned area. For example, convection-permitting simulations have suggested that convective outflows producing gust fronts may affect fire behavior in the Pantanal wetland, leading to rapid spread and large burned areas (Couto et al., 2024c, 2025a). Furthermore, changes in the large and mesoscale circulation along days can also lead to an erratic and unpredictable expansion of the fire front, such as verified in large fires occurring in southern Portugal (Purificação et al., 2024, 2025).

The present study is based on the premise that fire behavior over several weeks can vary considerably due to changes in the synoptic circulation. To evaluate this hypothesis, a set of fire–atmosphere coupled simulations are used to explore fire behavior on three different days over the three weeks during which the megafire in the Serra da Estrela Natural Park was active. The simulations were designed to assess fire spread across complex terrain, the development of pyro-convection and related phenomena, and to explore how evolving weather conditions can affect fire behavior over extended periods.

The manuscript is structured as follows: Section 2 presents the study area, data and methodology, followed by the results in Section 3. The results are discussed in Section 4, followed by the limitations and challenges for the study in Section 5, and conclusions in Section 6.

2 | STUDY AREA, DATA AND METHODOLOGY

2.1 | Case study: August 2022

Serra da Estrela, in central mainland Portugal (Figure 1a), straddles the Euro-Siberian and Mediterranean biogeographical regions. Although it covers just 1% of Portugal, the Natural Park is a key area, supporting one-third of the national flora, high plant endemism and a rich assemblage of vertebrate and invertebrate fauna. Designated a Natura 2000 priority site (Evans, 2012; Silva et al., 2019), the region now faces increasing threats – climate change, rural abandonment and fuel accumulation (Jansen, 2011; Moreira et al., 2010; Nunes et al., 2021).

In August 2022, a fire ignited in Garrocho burned over 20,000 ha (25% of the park) across 22 parishes in 20 days. This region has a documented history of significant fire events, notably those occurring in 1975, 1978, 2000, and 2017 (Lusa, 2022). Steep terrain, extreme fire weather conditions, and operational challenges (including poor helicopter maneuvering near the active front) exacerbated

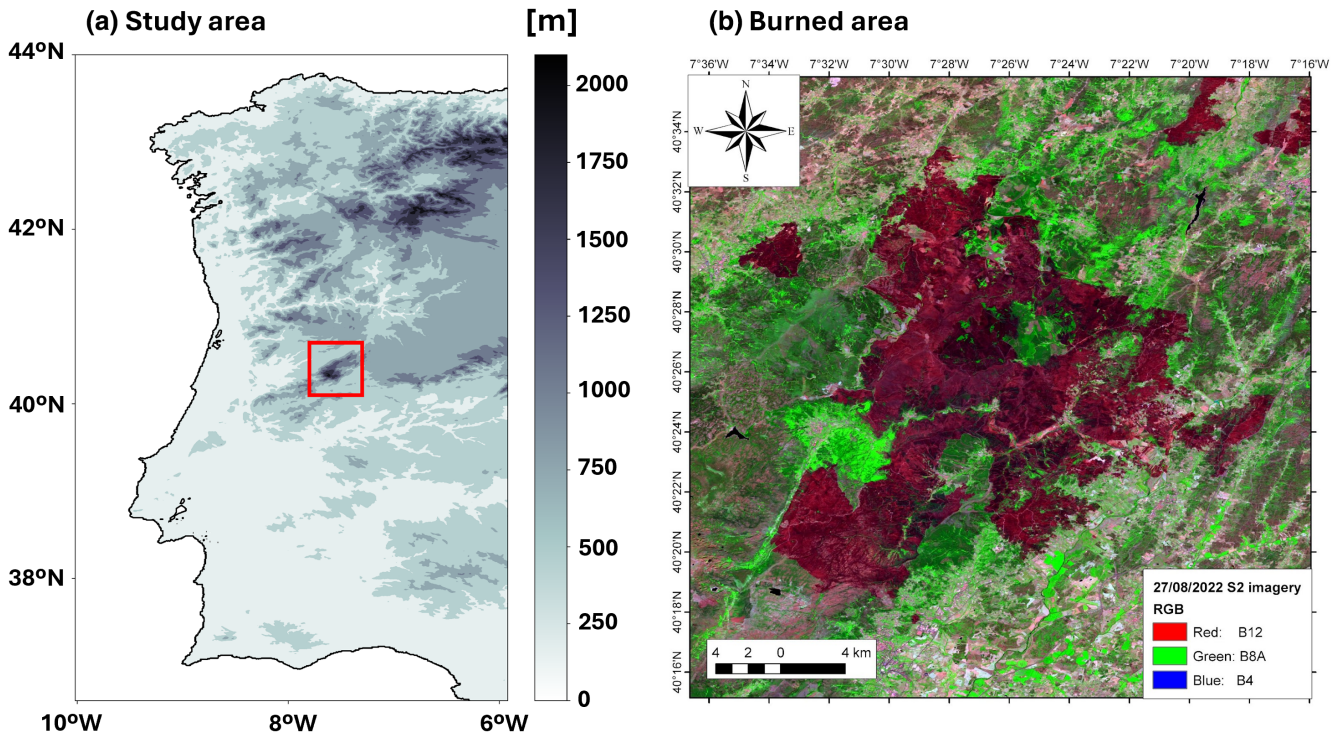

FIGURE 1 (a) Study area, the red square indicates the Serra da Estrela region and (b) the final burn area (pink shaded) obtained from Sentinel-2 imagery dated 27 August 2022. [Colour figure can be viewed at wileyonlinelibrary.com]

its spread (Mendonça et al., 2023), underscoring the urgent need for integrated land-management strategies. Figure 1b presents a false-color RGB composite from Sentinel-2 imagery on 27 August 2022, illustrating the final extent of the affected area throughout Serra da Estrela.

2.2 | Observation data

Table 1 below describes the observed data used in this study. It used data from four surface weather stations provided by the Portuguese Institute for Sea and Atmosphere (IPMA), located within the study area (Figure S1). The hourly data from the weather stations were used for a point-to-point validation of the numerical simulations. Large-scale atmospheric conditions were taken from the operational archive of the European Centre for Medium-Range Weather Forecasts (ECMWF), using the Meteorological Archival and Retrieval System (MARS), at a horizontal resolution of 0.125×0.125 degrees.

Weather radar data from the Arouca/Pico do Gralheiro (A/PG RADAR) dual-polarization system were used in this study, specifically the correlation coefficient (Rho_HV) field. This parameter measures the variability in the shapes, sizes, and orientation of targets within the atmospheric volumes scanned by the radar beam. Lower values indicate greater variability, whereas higher values correspond to more uniform characteristics. Typically, hydrometeors such as rain, snow, or ice crystals are more uniform in shape, size, and orientation than, for instance, smoke particles, and are therefore characterized by higher Rho_HV values. Rho_HV thus helps distinguish meteorological targets from smoke, with values exceeding 0.9 indicating condensed hydrometeors, and values below 0.6 typically associated with smoke (Pinto et al., 2022a).

Active Fire (AF) products derived from the Moderate Resolution Imaging Spectroradiometer (MODIS), and the Visible Infrared Imaging Radiometer Suite (VIIRS) sensors were used. Both AF products were retrieved from the National Aeronautics and Space Administration (NASA) Fire Information for Resource Management System (FIRMS) to assess the wildfire's temporal evolution.

2.3 | Numerical modeling

This fire event was studied using numerical modeling with the MesoNH atmospheric model and the ForeFire fire propagation model. The two models were coupled considering two-way interactions, in which the heat and vapor generated by the fire are injected into the atmosphere, while the near- surface wind drives the fire spread. Six numerical simulations were conducted (Table 2).

The Non-Hydrostatic Mesoscale atmospheric model (MesoNH) is a state-of-the-art limited-area model (Lac et al., 2018) with non-hydrostatic dynamics and a set of parameterizations that solve physical processes in the atmosphere including shallow and deep convection, turbulence, cloud microphysics and radiation transfer. Atmosphere–surface interactions are modeled using SURFEX (Masson et al., 2013), a platform that includes models for different surface types. The model has previously been used to study atmospheric conditions associated with the development of fires in Portugal (e.g., Couto et al., 2022, 2025b; Purificação et al., 2024, 2025). ECMWF

TABLE 1 Observed data used in this study.

Data			Data retrieved	Temporal	Spatial
Weather stations	Guarda (40.53° N, −7.28° W) Penhas Douradas (40.41° N, −7.56° W) Aldeia do Souto (40.35° N, −7.39° W) Covilhã (40.26° N, −7.48° W)		10-m wind gusts ($m \cdot s^{-1}$); 2-m air temperature (°C); 2-m relative humidity (%)	1 h	–
Synoptic charts	ECMWF		Wind ($m \cdot s^{-1}$) and geopotential fields ($m^2 \cdot s^{-2}$) at 850, 500, and 250 hPa	Once a day (1200 UTC or 1800 UTC)	0.125×0.125 degrees
Remote sensing data	Radar (40.85° N, 8.28° W)		Rho_HV	10 min (10 August 2022)	–
	Satellite	AQUA/TERRA MODIS	AF products	06/10/15 August 2022	1 km
		NPP/NOAA-20 VIIRS			375 m

Note: The table presents the dataset retrieval date, along with the temporal and spatial resolutions of each product.

TABLE 2 Main features of simulations.

Simulation					Start	Coupled	Ignition	End
Coupled simulations	MesoNH + ForeFire	EXP1 [IGN]	Ignition	–	5 August 2022 1800 UTC	6 August 2022 0000 UTC	6 August 2022 0220 UTC	6 August 2022 1200 UTC
		EXP2 [PYRO]	Pyro-Clouds	EXP2.1	10 August 2022 0000 UTC	10 August 2022 0600 UTC	10 August 2022 0630 UTC	10 August 2022 1800 UTC
				EXP2.2	10 August 2022 0600 UTC	10 August 2022 1200 UTC	10 August 2022 1230 UTC	11 August 2022 0000 UTC
		EXP3 [REACT]	Reactivation	–	15 August 2022 0600 UTC	15 August 2022 1200 UTC	15 August 2022 1447 UTC	15 August 2022 1800 UTC
Not coupled	MesoNH	CTR	Control EXP2	CTR2.1	10 August 2022 0000 UTC	–	–	10 August 2022 1800 UTC
				CTR2.2	10 August 2022 0600 UTC	–	–	11 August 2022 0000 UTC

Note: The table lists the name assigned to each simulation, starting time, coupling time between the models, fire ignition time, and the end of the simulation.

operational analyses, updated every six hours, were used as initial and boundary conditions.

ForeFire (Filippi et al., 2009) is a fire propagation model that can be coupled to the MesoNH model. This fire model enables simulation of the propagation of the fire front, and the computation of energy and mass fluxes emitted from the fire into the atmosphere. ForeFire has previously been successfully tested in several events in Portugal (Campos et al., 2023; Couto et al., 2024a,b).

In the two-way MesoNH/ForeFire coupling version (Filippi et al., 2009), fire–atmosphere interactions are modeled as follows: the atmospheric model drives the fire propagation model by providing values for the surface wind field at the first model level; In turn, the ForeFire model calculates the sensible and latent heat fluxes and the radiant temperature that are imposed at the first level of the MesoNH atmospheric model. Currently, smoke is treated as a passive scalar, with a constant release rate of 1 $m^2 \cdot s^{-1}$ over the burning area (Filippi et al., 2018) and, despite being sent to MesoNH, does not interact with the atmospheric environment, and hence is used exclusively to visualize the plume. The fuel map used was derived from Malinowski et al. (2020), who produced land cover/use maps for Europe based on Sentinel-2 imagery and a random forest classification approach. The resulting dataset provides 10-m resolution information and distinguishes 13 land cover classes.

2.3.1 | Simulations

The numerical experiments were done in three relevant periods of the Serra da Estrela fire event, which are identified as EXP1 [IGN], EXP2 [PYRO] and EXP3 [REACT] (Table 2). EXP1 [IGN] includes the ignition phase on 6 August; EXP2 [PYRO] comprises the period in which the development of pyro-convective clouds has been documented, on 10 August; and EXP3 [REAC] concerns the period of fire reactivation on 15 August. Due to computational constraints, two simulations were performed for 10 August in order to cover the entire diurnal cycle: one during the morning of the fire ignition – EXP2.1 [PYRO]; and the other in the early-afternoon ignition moment – EXP2.2 [PYRO]. In addition to these four coupled simulations, two additional control simulations (CTR) were done for EXP2 [PYRO] using only the MesoNH atmospheric model, keeping the same atmospheric configuration as in the coupled experiment, but without activating the fire model.

Table 2 presents the main features of each simulation, including the start, coupling, and end times, along with fire ignition point details. For EXP1 [IGN] (6 August, day of ignition) and EXP3 [REAC] (15 August, fire reactivation), ignition points, defined by coordinates and time, were selected to match observed fire fronts based on official reports (fogos.pt., 2022; Mendonça et al., 2023). On 10 August (EXP2 [PYRO]), the fire had already been active since 6 August and in order to identify a plausible ignition point, this study used satellite data from FIRMS/NASA, to find an ignition point for the model.

The domains considered in the simulations are shown in Figure 2. MesoNH was configured with three nested two-way domains, with horizontal resolutions of 1500 m (D1), 500 m (D2), and 250 m (D3), each consisting of 150 grid points (Figure 2a). The vertical grid consisted of 50 model levels, with the lowest level at 30 m above the surface and the highest at 900 m at the top.

The turbulence 3D scheme (Redelsperger & Sommeria, 1981) was activated for the inner domains (Figure 2), allowing the computation of horizontal and vertical flows, while for the outer domain (Figure 2), the turbulence was

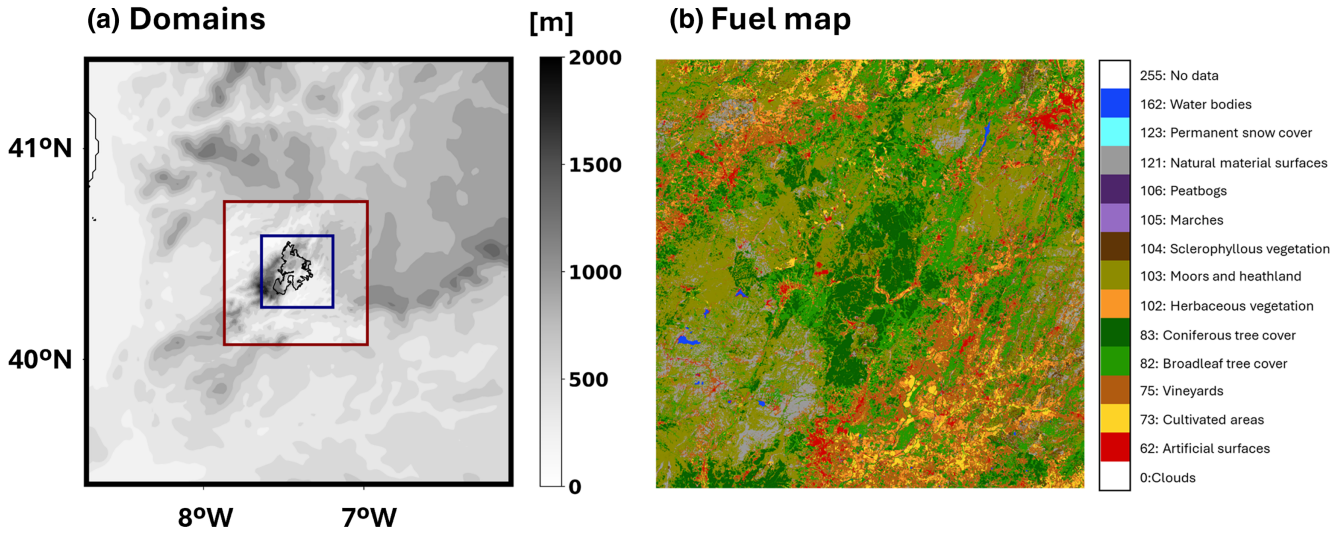

FIGURE 2 Horizontal configuration of the simulations: (a) horizontal configuration of MesoNH model. The outer domain at 1500 m (D1-black); the intermediate domain at 500 m (D2-red) and the innermost domain at 250 m (D3-blue), and (b) fuel map used in ForeFire model, obtained from Malinowski et al. (2020). The fire perimeter (black contour) in panel (a) was obtained from ICNF (2025). [Colour figure can be viewed at wileyonlinelibrary.com]

defined in 1D mode (Cuxart et al., 2000). The parameterization of cloud microphysics (ICE3) allows for the representation of five types of hydrometeors (Pinty & Jabouille, 1998). The radiation scheme was based on the Rapid Radiative Transfer Model (Mlawer et al., 1997) and in all simulations convection was assumed to be explicit.

ForeFire was coupled to the innermost model (D3), with fire model outputs requested at a high temporal resolution of 10 s. Unlike in previous studies, in which a uniform fuel map was considered (Campos et al., 2023; Couto et al., 2024a,b), in the present study, a non-uniform fuel map with 15 fuel classes (Malinowski et al. (2020); Figure 2b) was used, allowing for the differentiation of various vegetation types and other surface features (e.g., roads, rocks). In all experiments, the ForeFire model has been configured to release 0.005 kg of water vapor and generate a heat flow of 50,000 $W \cdot m^{-2}$ into the atmosphere along the advancing fire front, for a "burn duration" of 200 s. The grid resolution of ForeFire was set to 10 m with 3800×3800 grid points.

2.4 | Model verification

The model verification was performed using in situ data, radar and satellite. The near-surface meteorological variables are presented in Figures S2–S5 based on point-to-point validation. In all experiments, the model captured well the evolution of the 2-m air temperature with some underestimations, particularly during morning periods. Regarding humidity, the model reproduced reasonably well overall the variations in the 2-m relative humidity. Some overestimations were noted in Penhas Douradas and Aldeia do Souto (especially in EXP2.1 [PYRO] and EXP3 [REAC]) while some underestimations occurred in Guarda and Covilhã stations (evening in EXP2.2 [PYRO]). The model generally underestimated the 10-m wind gusts in experiments EXP1 [IGN], EXP2.1 [PYRO] and EXP2.2 [PYRO]. On the other hand, in EXP3 [REAC], the model tended to overestimate wind gusts across the stations. A complete description may be found in the Supporting information.

The validation of the simulated pyro-convective clouds was performed using radar, and is presented in Section 3.2.2. The fire model was validated using satellite data (AF products), presented in Section 3.2.4.

3 | RESULTS

3.1 | Large-scale environment

This section provides an overview of the synoptic patterns in the three periods under study. Figure 3a–c represents 6 August, Figure 3d–f represents 10 August, and Figure 3g–i represent 15 August. The first column shows wind field (speed and direction) and geopotential field at the 850-hPa level. The second and third columns present the same variables, but at 500 and 250-hPa levels, respectively.

Figure 3a shows a high-pressure center on 6 August positioned northwest of Portugal, extending towards the British Isles. A low-pressure system centered westward of the Iberian Peninsula is observed in the geopotential height field at 850 hPa, which induces a south/

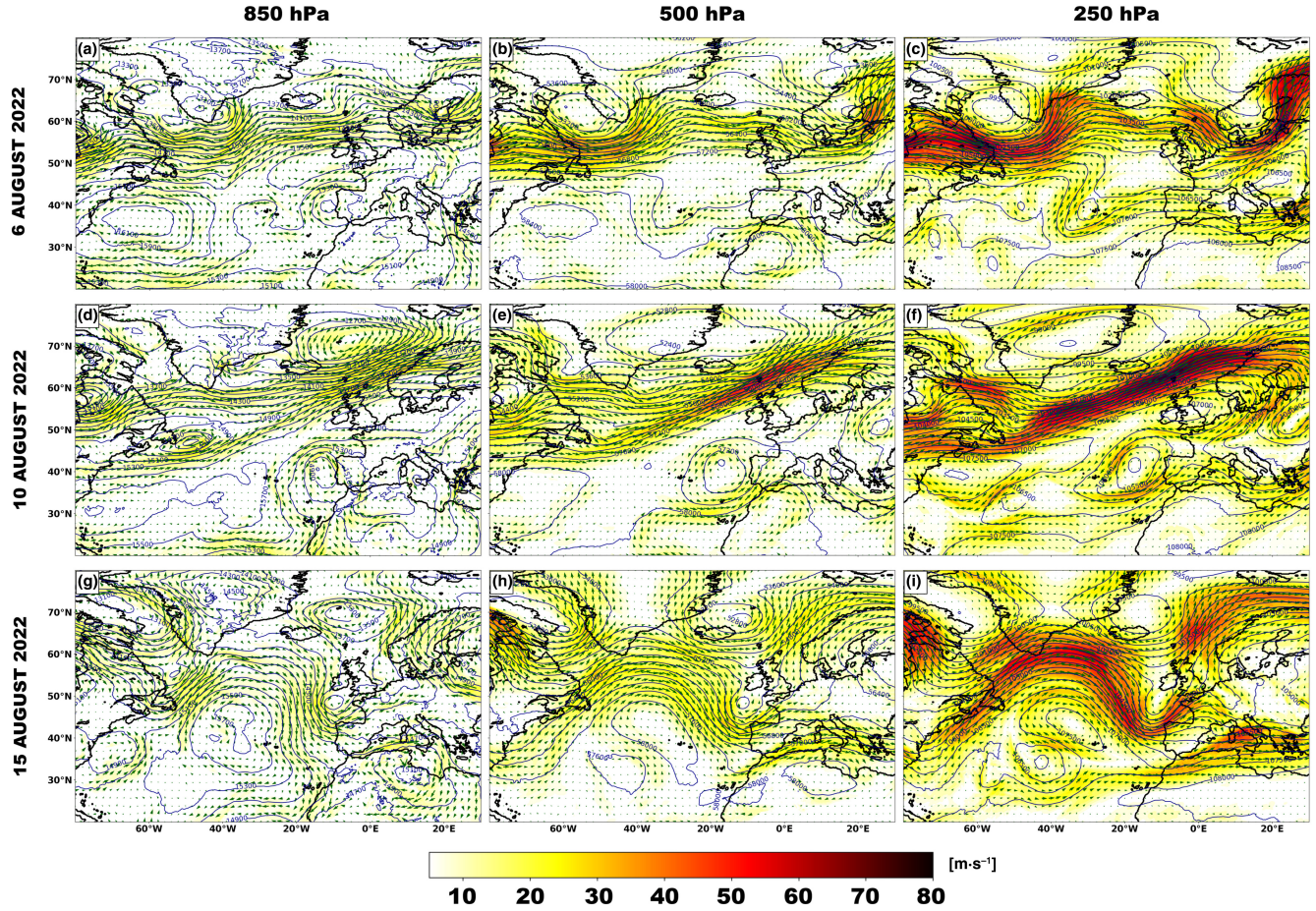

FIGURE 3 Wind field, speed ($m \cdot s^{-1}$, shaded areas) and direction (arrows): (a–c) 6 August 2022 1200 UTC, (d–f) 10 August 1200 UTC, and (g–i) 15 August 2022 1800 UTC. Columns represent the wind field at different levels, namely 850 hPa (left), 500 hPa (middle), and 250 hPa (right). [Colour figure can be viewed at wileyonlinelibrary.com]

southwesterly wind over the Iberian Peninsula (Figure 3a). This circulation contributes to the advection of warm and dry air from North Africa to the Iberian Peninsula (not shown). In the 500 hPa geopotential height field, the weak flow over Portugal is predominantly southwesterly (Figure 3b). Westerly winds are identified over the Iberian Peninsula in Figure 3c. The same figure also shows a trough over the Azores Archipelago (39° N, 30° W), which is found configuring an upper low-pressure core at 250 hPa (Figure 3c).

On 10 August (Figure 3d), a low-pressure system at 850 hPa was found centered west of Portugal, approximately at 40° N and 14° W. It is noteworthy to mention that this system is not exactly the same low-pressure identified on 6 August. Its development started on 7 August at the upper levels and northwest of the Iberian Peninsula (not shown) and deepened to configure the cyclonic circulation identified at 850 hPa, which induced southwesterly winds at the same level over Portugal (Figure 3d). A more intense low-pressure system is found at upper levels, namely at 500 hPa (Figure 3e) and 250 hPa (Figure 3f). The vertical axis of the cyclone's upper level is slightly tilted westward relative to the cyclone at 850 hPa. This low-pressure system continues its development in the following days, starting its dissipation stage as it moves northeastwards (not shown).

On 15 August, Figure 3g displays the Azores anticyclone located over the Atlantic Ocean at 850 hPa, whereas over the western Iberian Peninsula a distinct circulation emerges compared to the previous days, with winds blowing from northwesterly/westerly (Figure 3g). At the upper levels, a trough is visible approaching Portugal from the northwest (Figure 3h,i). The positioning of this cut-off low over the Bay of Biscay produced predominantly westerly winds over the north Iberian Peninsula.

3.2 | Coupled simulations

3.2.1 | EXP1 [IGN]: 6 August 2022

The atmospheric model, without coupling, is initialized from the ECMWF analysis at 1800 UTC on 5 August 2022. The fire propagation model is coupled and activated at

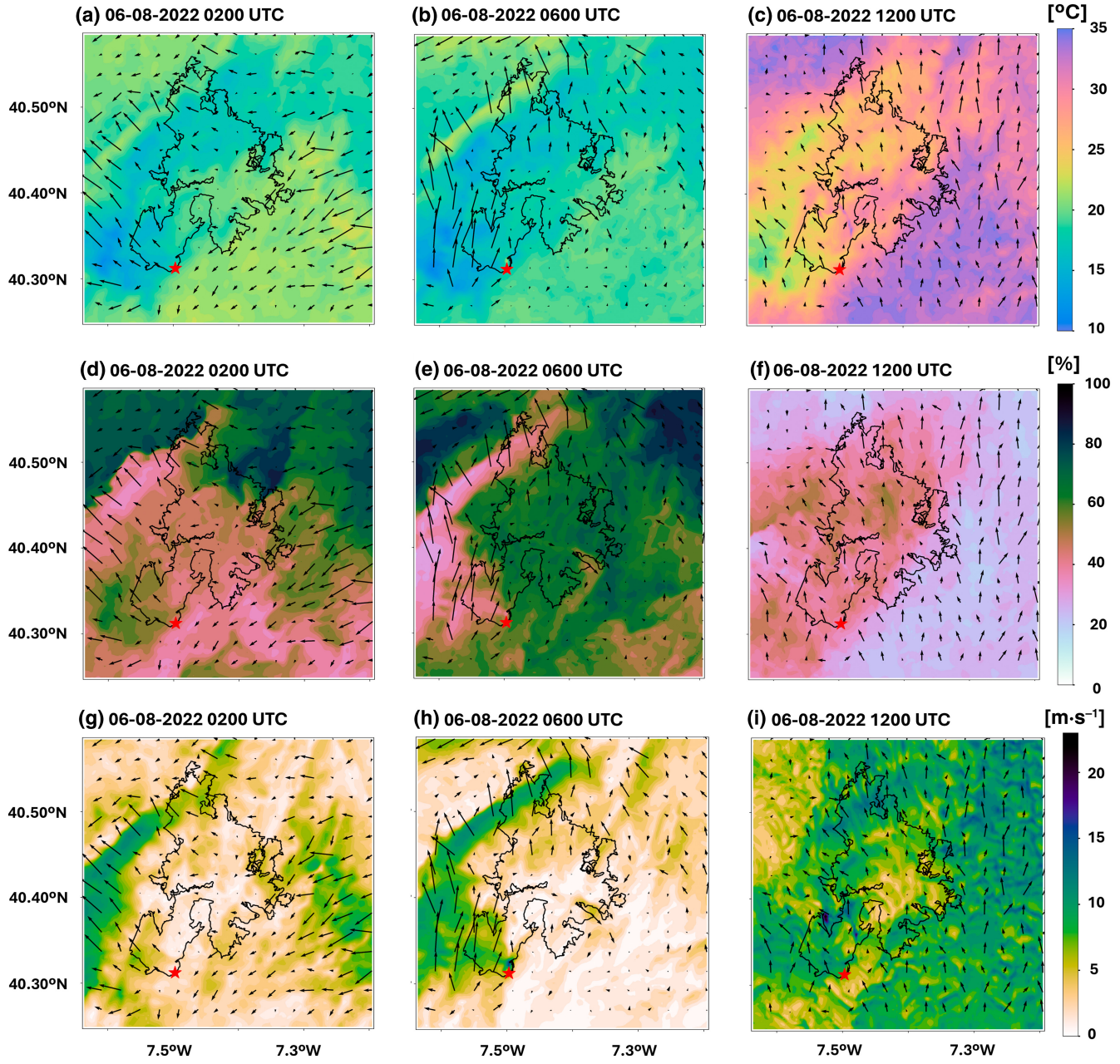

FIGURE 4 Fire weather variables: (a–c) temperature at 2 m (shaded, °C) and wind at 10 m (vectors, $m \cdot s^{-1}$); (d–f) humidity at 2 m (shaded, %) and wind at 10 m (vectors, $m \cdot s^{-1}$); (g–i) gusts at 10 m (shaded, $m \cdot s^{-1}$) and wind at 10 m (vectors, $m \cdot s^{-1}$) on 6 August 2022. The fire perimeter (black contour) was obtained from ICNF (2025). [Colour figure can be viewed at wileyonlinelibrary.com]

0000 UTC on 6 August, and the fire is introduced at 0220 UTC (Table 2), since ignition occurred at 0218 UTC on 6 August 2022 (fogos.pt., 2022).

Figure 4 shows fire-related weather variables. Nighttime temperatures range from 10°C to 22°C, with lower temperatures occurring at higher elevations. As dawn approaches, temperatures begin to rise, exceeding 30°C in some regions at 1200 UTC (Figure 4a–c). Relative humidity evolves inversely to temperature. During the night the relative humidity is higher, especially in the northwest and northeast areas of the domain. At the end of the simulation, 1200 UTC, in most of the domain the humidity is below 40% (Figure 4d–f). The simulation indicates the existence of strong wind gusts from the Southeast during the night, highlighting orographic effects. From 0900 UTC, wind gusts increase across the region (not shown). As expected, the highest mountainous areas present the highest gust values (Figure 4g–i).

In addition, the entire figure shows that the presence of mountains in the region causes an increase in temperatures on the leeward side (Figure 4b), consistent with the decrease in relative humidity (Figure 4e) due to

adiabatic heating. While this effect does not directly influence fire spread, strong gusts are still simulated in the fire area at 1200 UTC (Figure 4i).

Figure 5 illustrates the turbulence field near the surface (model first level) (shaded areas, $m^2 \cdot s^{-2}$), the 10-m wind and the smoke variable near the surface (contour, dimensionless), which was plotted at a threshold of 0.01. The south/southeasterly wind pushed the fire front northwestward (Figure 5a,b). The highest turbulence values are above the fire front, with values around 8 $m^2 \cdot s^{-2}$. The largest wind vectors, indicating higher intensities, align with the orography and appear to influence the fire front's development, as it spreads toward the northwest. Also, high values of turbulence outside the fire domain highlight the interaction between topography and the atmospheric flow (not shown). The model simulated the fire front moving north during the initial hours (Figure 5a,b) and, from 0900 UTC, the fire front became larger and propagated northwestward (Figure 5c,d).

Figure 6 depicts two vertical cross-sections (south–north) identified in Figure 5c,d, illustrating turbulence (Figure 6a,b) and vertical velocity (Figure 6c,d). Cross-sections were chosen to intersect regions of maximum turbulence along the fire front. The simulation indicates that the highest air turbulence values occur over the fire (Figure 6a,b). The highest values were reached at 1200 UTC, with turbulence ranging between 7 and 8 $m^2 \cdot s^{-2}$, with the convective column reaching an altitude of about 3000 m (Figure 6b). The fire induces vertical upward motions as seen in Figure 6c,d. At 1200 UTC, an upward current of 8 $m \cdot s^{-1}$ was simulated to occur over the fire (lighter-shaded areas, Figure 6d). A downdraft (indicated by the darkest shading) is evident in the figure just ahead of the fire-induced updraft. Other less intense updrafts and downdrafts in the figure highlight the interaction of the southerly current with the orography, which is also likely to be affected by the ongoing fire itself.

3.2.2 | EXP2 [PYRO]: 10 August 2022

Figure S6 shows two satellite images taken on the same day during the two satellite overpasses over mainland Portugal, highlighting active-fire spots (marked in orange), fire plumes (smoky areas), and cloud cover (white). Figure S6a corresponds to the TERRA satellite's morning pass around 1100 UTC while Figure S6b corresponds to the AQUA satellite's afternoon pass around 1400 UTC. The presence of cumulus clouds in Figure S6b shows that there were favorable conditions for daytime atmospheric instability.

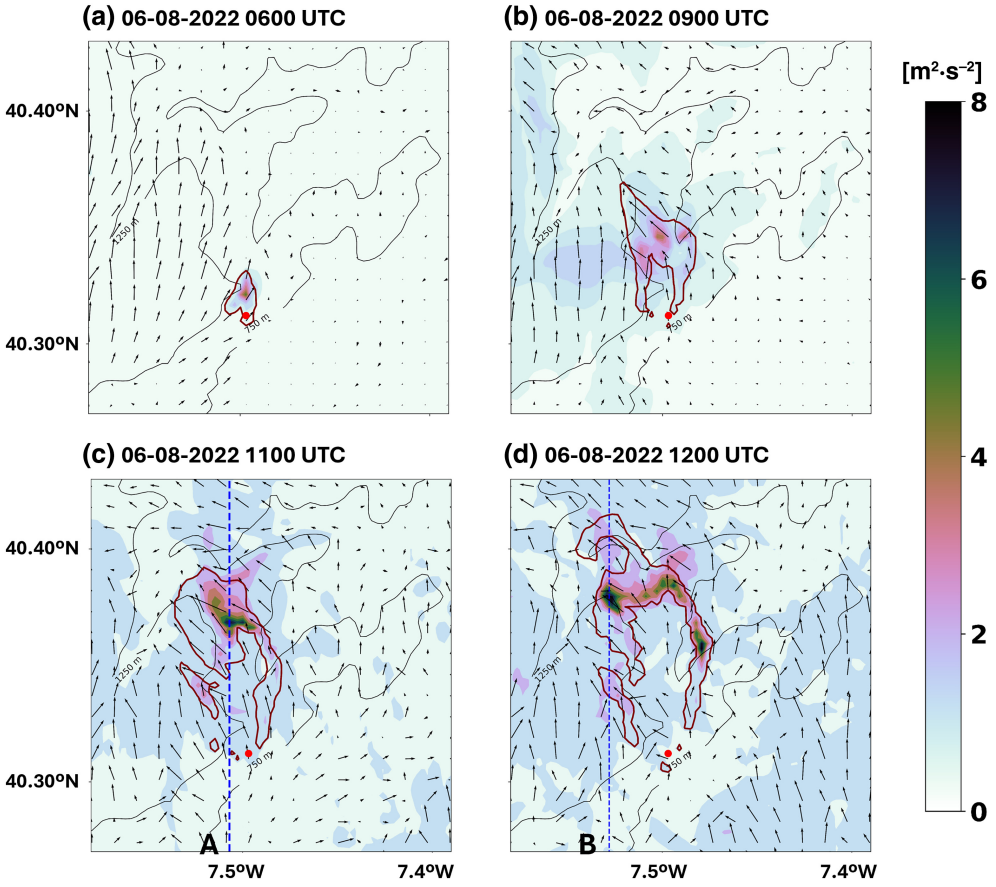

FIGURE 5 Zoomed into the fire area: turbulence field near surface (shaded, $m^2 \cdot s^{-2}$), winds at 10 m (arrows, $m \cdot s^{-1}$), smoke variable thresholded at 0.01 near surface (red contour, dimensionless), orography (black contours, m) at: (a) 0600 UTC, (b) 0900 UTC, (c) 1100 UTC and (d) 1200 UTC on 6 August 2022. The dashed lines (A, B) represent cross-section locations. Red dot represents fire ignition simulated on 6 August 2022 (see Table 2). [Colour figure can be viewed at wileyonlinelibrary.com]

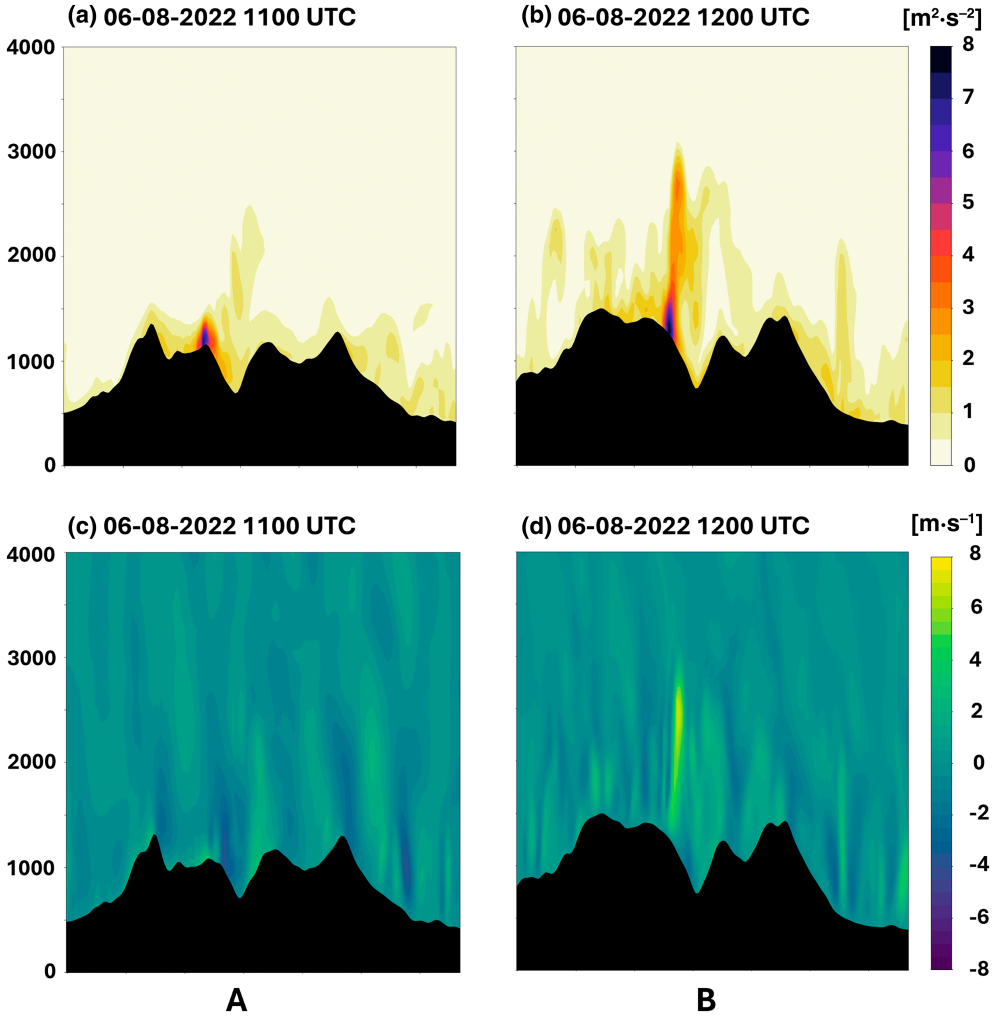

FIGURE 6 Vertical cross-section (south–north) under lines A and B shown in Figure 5: (a,b) turbulence field ($m^2 \cdot s^{-2}$) and (c,d) vertical velocity ($m \cdot s^{-1}$) at two time points – 1100 UTC and 1200 UTC on 6 August 2022. [Colour figure can be viewed at wileyonlinelibrary.com]

Figures 7 and 8 show the radar data for two selected periods, showing the vertical cross-sections across the plume derived from radar observations. Figure 7a–d corresponds to EXP2.1 [PYRO] (Part I), while Figure 8a–d refers to EXP2.2 [PYRO] (Part II). Line A–B represents the cross-section across the plume. Although the hotspot is not precisely located at point 'A', the plume pattern indicates that its position is in close proximity. Starting at 1340 UTC on 10 August 2022 (Figure 7a), higher Rho_HV values (depicted in yellow/lighter-shaded areas) begin to appear above the plume, which generally remains characterized by lower Rho_HV values (identified in green/darkest shading), except for an area near point B, at the northern end of the section. These later high values are attributed to ground clutter contamination. This vertical structure suggests condensation or glaciation at higher altitudes and a persistent pure smoke plume at lower levels. Over the following 30 min, the glaciated region descends slightly and is advected northward (Figure 7b–d). Despite this advection, it remains connected to the underlying smoke plume that was generated by the fire. In the second observation period (Figure 8a–d), higher Rho_HV values are detected at 1700 UTC on 10 August (Figure 8a), peaking at 1730 UTC (Figure 8b), with smoke observed between zones of condensed material (yellow colors/lighter-shaded regions). Both observational sequences confirm the presence of condensed material atop the fire plume, indicating pyrocumulus cloud formation.

As previously mentioned, simulations were run to assess the model's ability to reproduce fire-induced cloud development. Figure 9 illustrates evolution of the fire front for the two numerical experiments, EXP2.1 [PYRO] (Figure 9a–d) and EXP2.2 [PYRO] (Figure 9e–h), using the same variables as in Figure 5. In EXP2.1 [PYRO], during the morning (Figure 9a,b), maximum turbulence values (4–5 $m^2 \cdot s^{-2}$) occur over mountainous terrain, with wind driving the fire front westward. After 1200 UTC, turbulence intensifies and the fire front shifts north and northwestward (Figure 9c,d). In EXP2.2 [PYRO], initial southerly winds drive the fire front northward at 1700 UTC (Figure 9e). However, by 1900 UTC (Figure 9f), a shift to westerly winds directs the fire spread eastward (Figure 9f,g) and the highest turbulence values

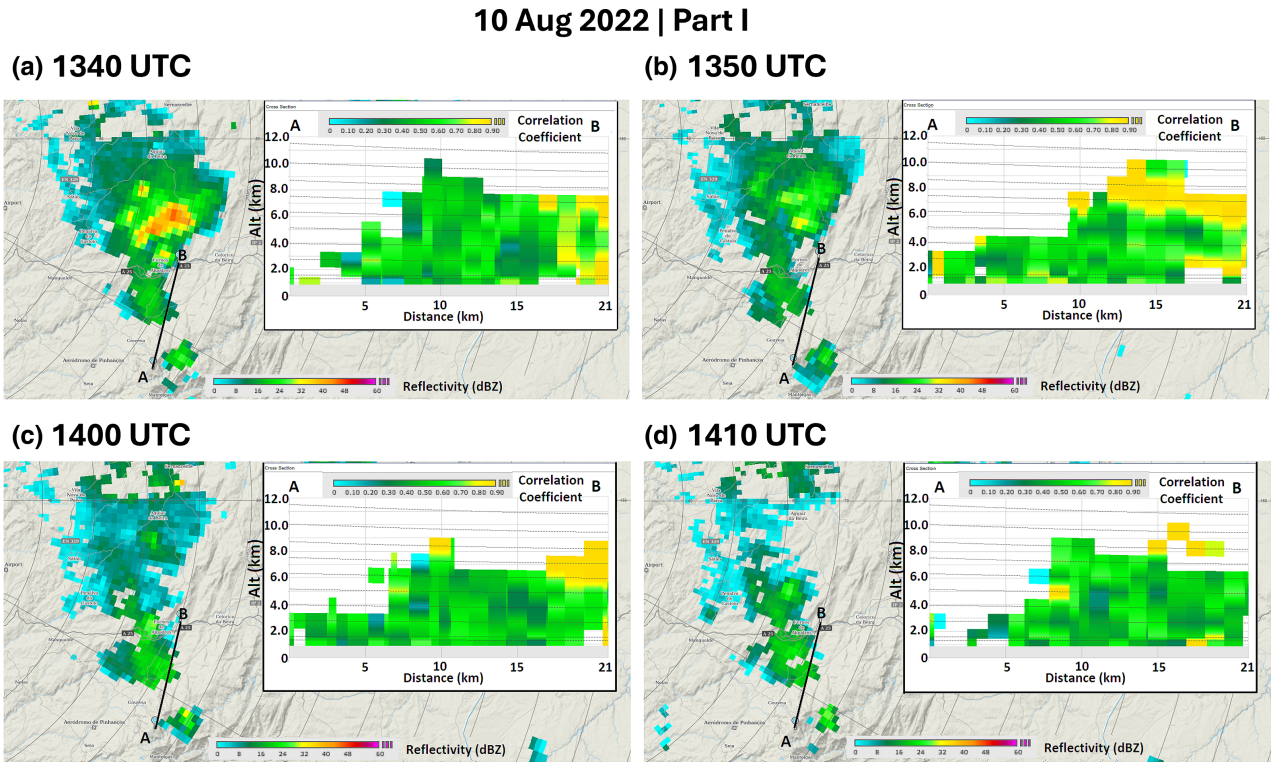

FIGURE 7 Plane position indicator (PPI) of radar reflectivity (low elevation) in horizontal projection (units: dBz) and vertical section of correlation coefficient (adimensional), inserted at each indicated time, August 10, 2022,A/PG RADAR. A vertical section was applied over the black segment. Part I represents the EXP2.1 simulation. [Colour figure can be viewed at wileyonlinelibrary.com]

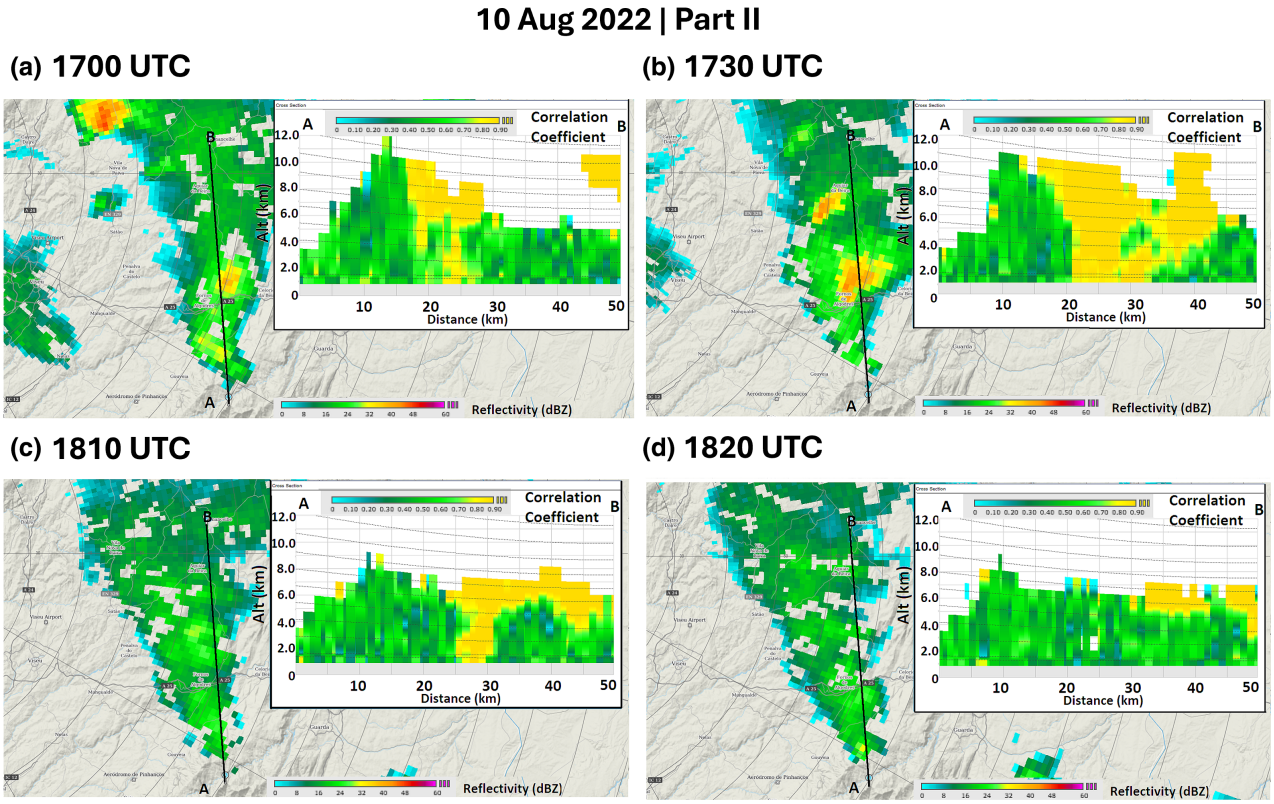

FIGURE 8 Plane position indicator (PPI) of radar reflectivity (low elevation) in horizontal projection (units: dBz) and vertical section of correlation coefficient (adimensional), inserted at each indicated time, August 10, 2022, A/PG RADAR. A vertical section was applied over the black segment. Part II represents the EXP2.2 simulation. [Colour figure can be viewed at wileyonlinelibrary.com]

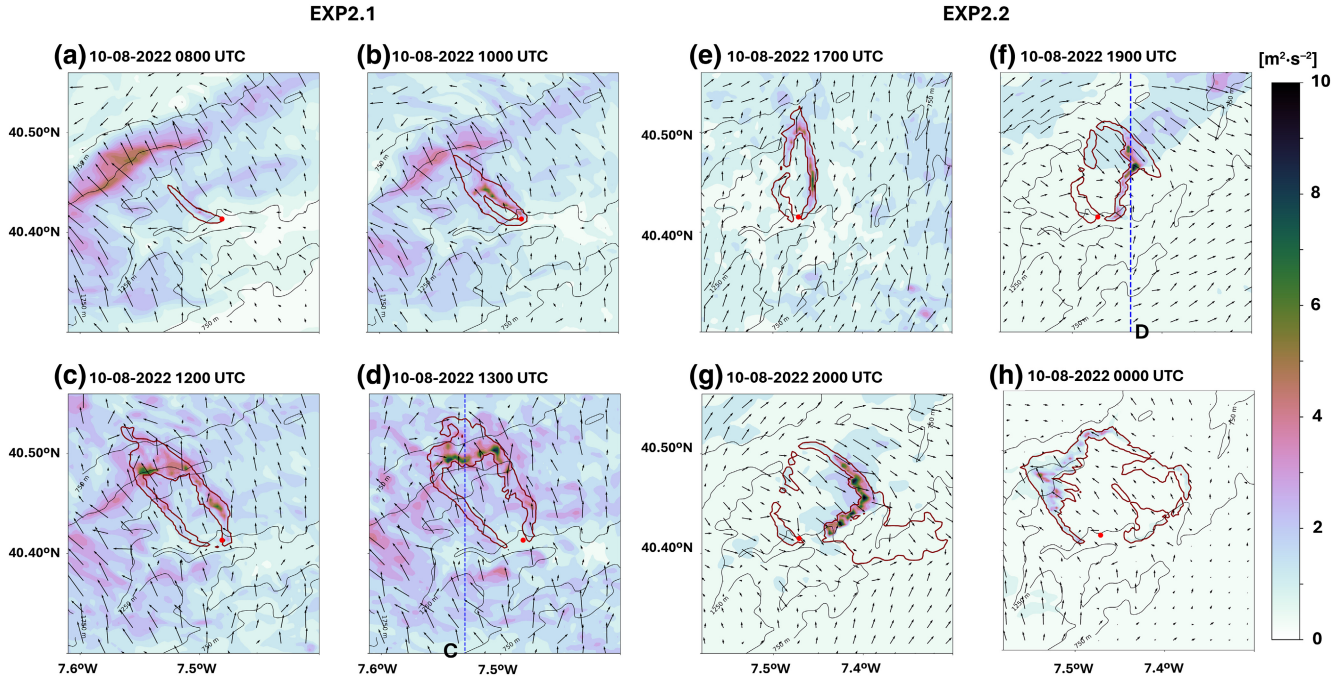

FIGURE 9 Zoomed into the fire area: turbulence field at surface (shaded, $m^2 \cdot s^{-2}$), winds at 10 m (vectors, $m \cdot s^{-1}$), smoke variable thresholded at 0.01 near surface (red contour, dimensionless), orography (black contours, m) for EXP2.1 [PYRO] experiment at: (a) 0800 UTC, (b) 1000 UTC, (c) 1200 UTC and (d) 1300 UTC on 10 August 2022, and for EXP2.2 [PYRO] experiment at: (e) 1700 UTC, (f) 1900 UTC, (g) 2000 UTC and (h) 0000 UTC on 10 August 2022. The dashed lines (c,d) represent cross-section locations. Red dot represents fire ignition simulated for 10 August 2022 (see Table 2). [Colour figure can be viewed at wileyonlinelibrary.com]

(9–10 $m^2 \cdot s^{-2}$) are observed near the fire front. From 2200 UTC onward, a further wind shift sustains the westward propagation (Figure 9h).

The two-dimensional field of vertically integrated hydrometeors is analyzed to assess the presence of hydrometeor concentrations within the innermost domain, particularly in the fire area (not shown). In both simulations, hydrometeor concentrations were observed at specific times near the fire area. Based on this analysis, vertical cross-sections (south–north) were plotted at these times to examine the pattern of the fields at higher altitudes. Figure 10 displays the vertical velocity field, turbulence, and total hydrometeor concentration, thus providing insight into the dynamic and microphysical structure of the pyro-convective event.

Figure 10a–c shows the results at 1300 UTC for EXP2.1 [PYRO] and Figure 10d–f shows the results at 1900 UTC for EXP2.2 [PYRO]. For EXP2.1 [PYRO] simulation, a slight turbulent vertical column is observed, with values ranging around 3 $m^2 \cdot s^{-2}$ (Figure 10a) and ascending velocities above 3 $m \cdot s^{-1}$ (Figure 10b), reaching altitudes of up to 4000 m. This vertical motion promoted condensation aloft, with a small core presenting hydrometeor concentrations of up to 0.8 $g \cdot kg^{-1}$ between 3000 and 3200 m (Figure 10c). In EXP2.2 [PYRO], stronger updrafts reached 7000 m, accompanied by turbulence values up to 20 $m^2 \cdot s^{-2}$ (Figure 10d) and vertical velocities of 20 $m \cdot s^{-1}$ (Figure 10e). Hydrometeor concentrations were significantly higher in this case, reaching 6 $g \cdot kg^{-1}$ at upper levels (Figure 10f), indicating intense convective development, and the formation of a pyro-convective cloud.

Thus, both experiments show evidence of condensation in altitude, though it was more pronounced in EXP2.2 [PYRO], which exhibited higher hydrometeor concentrations associated with an updraft exceeding 7000 m in altitude.

To assess whether cloud formation resulted from fire-induced processes, two control simulations (CTR2.1 and CTR2.2), one for each EXP2 [PYRO] subperiod, were performed using only the atmospheric model, with all other settings identical (Table 2). Figure S7 shows the same fields, in the same sections, at the same times as those shown in Figure 10 in order to facilitate comparisons. In both control runs, vertical velocity and turbulence were significantly weaker in the fire region, with no evidence of the strong updrafts seen in the coupled simulations; only boundary layer-driven motions were reproduced. Furthermore, no hydrometeors were detected at altitude in any of the cases. This leads to the conclusion that the formation of the clouds is a result of the impact of the fire on the atmosphere.

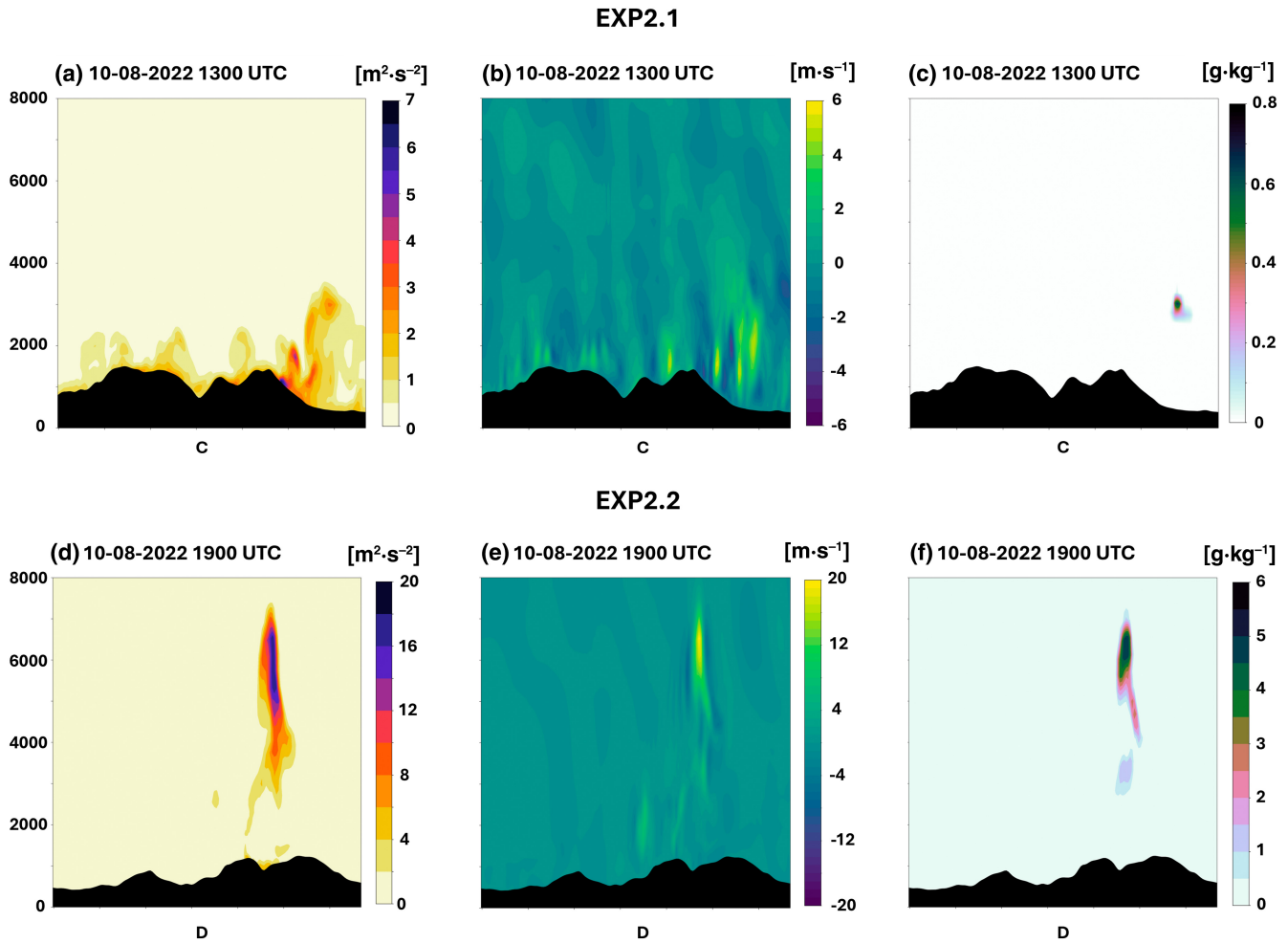

FIGURE 10 Vertical cross-section (south–north) under line C shown in Figure 9d for the EXP2.1 [PYRO] experiments over the variables: (a) turbulence field ($m^2 \cdot s^{-2}$), (b) vertical velocity ($m \cdot s^{-1}$) and (c) hydrometers concentration ($g \cdot kg^{-1}$) at 1300 UTC on 10 August 2022. Vertical cross-section (south–north) under line D shown in Figure 9f for EXP2.2 [PYRO] experiments over the variables: (d) turbulence field ($m^2 \cdot s^{-2}$), (e) vertical velocity ($m \cdot s^{-1}$) and (f) hydrometers concentration ($g \cdot kg^{-1}$) at 1900 UTC on 10 August 2022. [Colour figure can be viewed at wileyonlinelibrary.com]

3.2.3 | EXP3 [REAC]: 15 August 2022

According to Mendonça et al. (2023), the fire was declared "controlled" on 15 August, but a miscalculated helicopter maneuver reignited the fire. This simulation focuses on the reactivation observed around 1447 UTC in the Vale das Moreiras region (see Table 2 for details).

Figure 11 illustrates turbulence (shaded, $m^2 \cdot s^{-2}$) and 10-m wind (vectors, $m \cdot s^{-1}$). The front progresses eastward, with turbulence increasing over time (Figure 11b–d). The figures also show the presence of higher values of turbulence far from the ignition point, highlighting the important role of local orography. The westerly flow, with wind gust intensity increasing between 1600 and 1800 UTC, peaked at more than 20 $m \cdot s^{-1}$ over the fire area (Figure S8). A concurrent rise in humidity and a drop in temperature were also noted throughout the day (not shown).

Figure 12 shows the E vertical cross-section (west–east) (see Figure 11) of turbulence and vertical velocity fields at 1600 UTC and 1700 UTC. Turbulence maximums from the fire extend up to 2000 m, with peak values (8 $m^2 \cdot s^{-2}$) near the surface. The increase in turbulence is also aligned with strong updrafts in the vertical velocity field (lighter-shaded regions), reaching up to 7 $m \cdot s^{-1}$.

Figure S9 shows the water vapor field at four key time steps previously analyzed from each simulation. Concentration is higher near the surface and decreases with altitude, approaching zero, as expected, near the top of the atmosphere. Surface values exceed 11 $g \cdot kg^{-1}$ on 10 August 2022. In the case of intense pyro-convective activity (Figure S8c), a filament is seen penetrating the dry atmosphere, aligning with the previously identified pyro-convective cloud region.

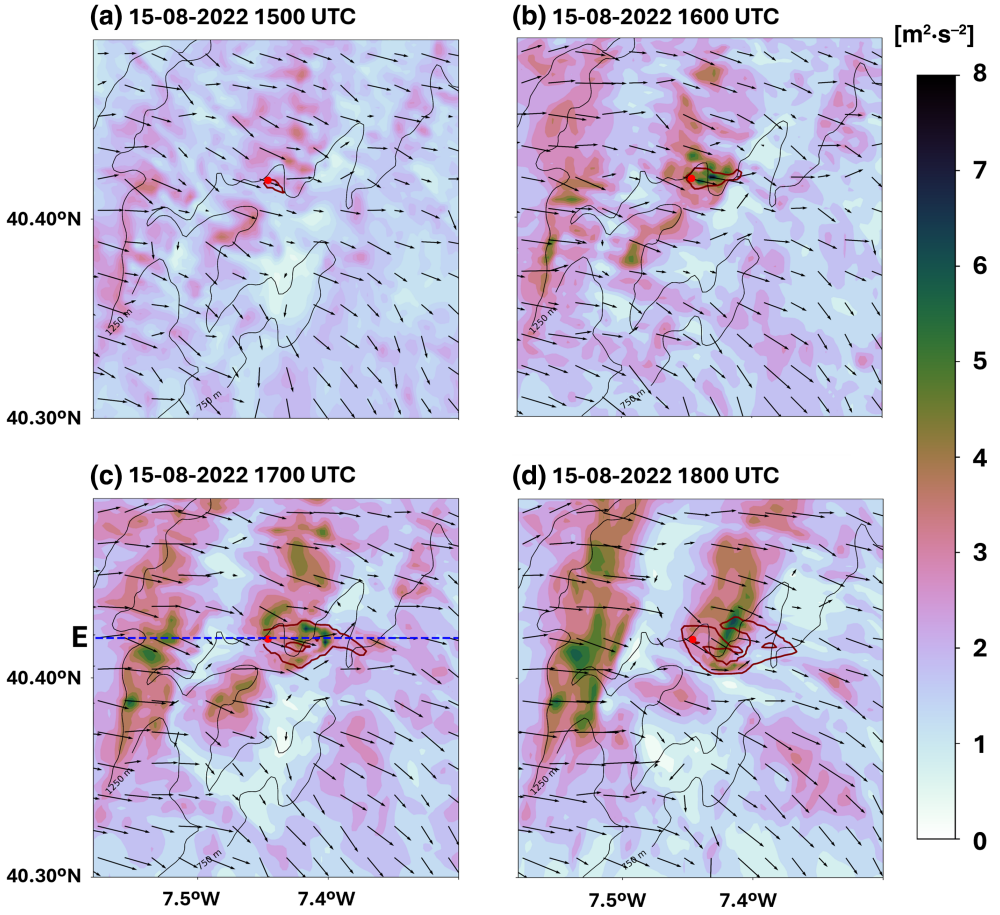

FIGURE 11 Zoomed into the fire area: turbulence field near surface (shaded, $m^2 \cdot s^{-2}$), winds at 10 m (vectors, $m \cdot s^{-1}$), smoke variable thresholded at 0.01 near surface (red contour, dimensionless), orography (black contours, m) at: (a) 1500 UTC, (b) 1600 UTC, (c) 1700 UTC and (d) 1800 UTC on 15 August 2022. The dashed line (E) represents the cross-section location. Red dot represents fire ignition simulated at 15 August 2022 (see Table 2). [Colour figure can be viewed at wileyonlinelibrary.com]

3.2.4 | Burned area: Model–observation comparison

To assess the agreement between simulated fire progression and ground truth, a visual intercomparison was made for each experimental phase. An RGB false-color composite derived from Sentinel-2 was used to highlight burned areas. Figure 13 shows the simulated fire spread with the ForeFire model (in blue color ramp) alongside all available AF product (triangles) detections for each date. As AF products represent instant moments, they do not capture subdaily fire evolution. Meteosat data were excluded due to low spatial resolution.

Figure 13a presents the simulation for the first day, 6 August 2022, showing a northward spread. However, AF data suggest the actual progression was toward the northwest, with continued burning still occurring in that direction on 7 August (indicated by black triangles), showing discrepancies between model and observation. Figure 13b,c corresponds to simulations for 10 August (EXP2.1 [PYRO] and EXP2.2 [PYRO], respectively), both aligning well with observed active-fire areas, though the model overestimated the extent of the burnd. Figure 13d shows the comparison of results for EXP3 [REAC]. The simulation shows that the fire spread eastward, in agreement with observations that show the fire developing in the same direction. However, due to unavailability of NOAA-20 (N20) sensor data on this date, the imagery relies on TERRA sensor data, which have a coarser spatial resolution.

4 | DISCUSSION

The Serra da Estrela fire broke out on 6 August 2022, devastating over 20,000 hectares. Given the fire's spatial extent and duration, computational constraints restricted the simulations to three key periods: 6 August (initial ignition), 10 August (pyro-convective cloud activity), and 15 August (intense reactivation).

According to IPMA, mainland Portugal was experiencing a severe meteorological drought in August 2022, marked by two heatwaves (29 July to 14 August and 20 to 29 August). The Palmer Drought Severity Index (PDSI) classified 60% of the territory under severe drought and 40% under extreme drought conditions (IPMA, 2022). Additionally, the Fire Weather Index (FWI) (Wagner, 1987) ranged between 30 and 40, indicating high to very high fire danger levels (IPMA, 2022). Both drought and fuel availability indices exceeded the 2000–2019 average.

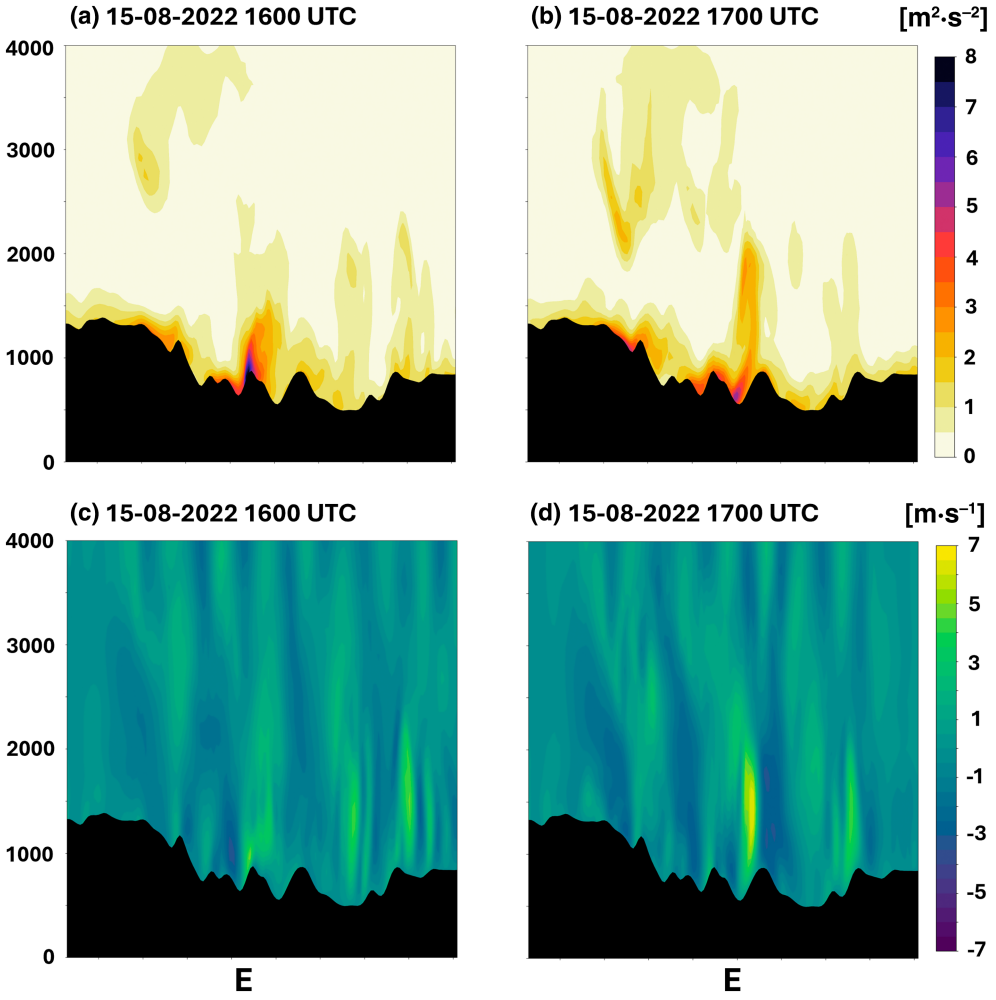

FIGURE 12 Vertical cross-section (west–east) under line E shown in Figure 11 over the variables: (a,b) turbulence field ($m^2 \cdot s^{-2}$) and (c,d) vertical velocity ($m \cdot s^{-1}$) at (a,c) 1600 UTC and at (b,d) 1700 UTC on 15 August 2022. [Colour figure can be viewed at wileyonlinelibrary.com]

The extended dry period led to reduced fuel moisture, further intensifying the fire activity (IPMA, 2022). Numerous studies have linked heatwaves and droughts to more frequent extreme wildfires worldwide (Hegedűs et al., 2024; Libonati et al., 2022; Mario et al., 2024; Nojarov & Nikolova, 2022; Pausas & Keeley, 2021; Ruffault et al., 2020). Parente et al. (2019) found a strong correlation between heatwaves and the timing and geographic distribution of extreme wildfires in Portugal.

In the larger-scale context, the study identified the development of low-pressure systems centered west of the Iberian Peninsula, initially observed only at lower levels (6 August) and, later (10 August), extending to the upper levels. In both patterns, south/southwesterly winds characterized the low-level flow over Portugal. The second scenario was recently highlighted configuring an atmospheric blocking system in early July 2022 (Couto et al., 2025b). The system's semistationary favored the advection of warm, dry air from North Africa, which maintained favorable fire-weather conditions in the Iberian Peninsula for several days. During the reactivation period (15 August), the approach of a trough and the development of a cut-off centered in the Bay of Biscay favored a strong northwesterly/westerly flow over the western Iberian Peninsula. At the regional scale, the simulation revealed a pattern of near-surface high temperatures and low relative humidity. Higher elevations had lower temperatures, which dropped overnight and remained lower until morning (EXP1 [IGN] and EXP2.1 [PYRO]). Daytime heating led to rising temperatures and further decreased relative humidity (EXP2.2 [PYRO] and EXP3 [REAC]). The wind gust field analysis revealed the highest wind gusts at night at higher altitude regions (e.g., EXP1 [IGN]).

The changes in the atmospheric circulation directly influenced fire spread intensity and direction along the event. On 6 August, the simulation indicated that the wind field favored spread toward the north/northwest. On 10 August, the two numerical experiments showed different scenarios: in the first, during the morning, the fire front continued moving northward, while the second experiment, during the afternoon, showed multiple directional changes, initially advancing to the north, then shifting to east, and later turning to west. On 15 August, the wind favored an eastward fire propagation.

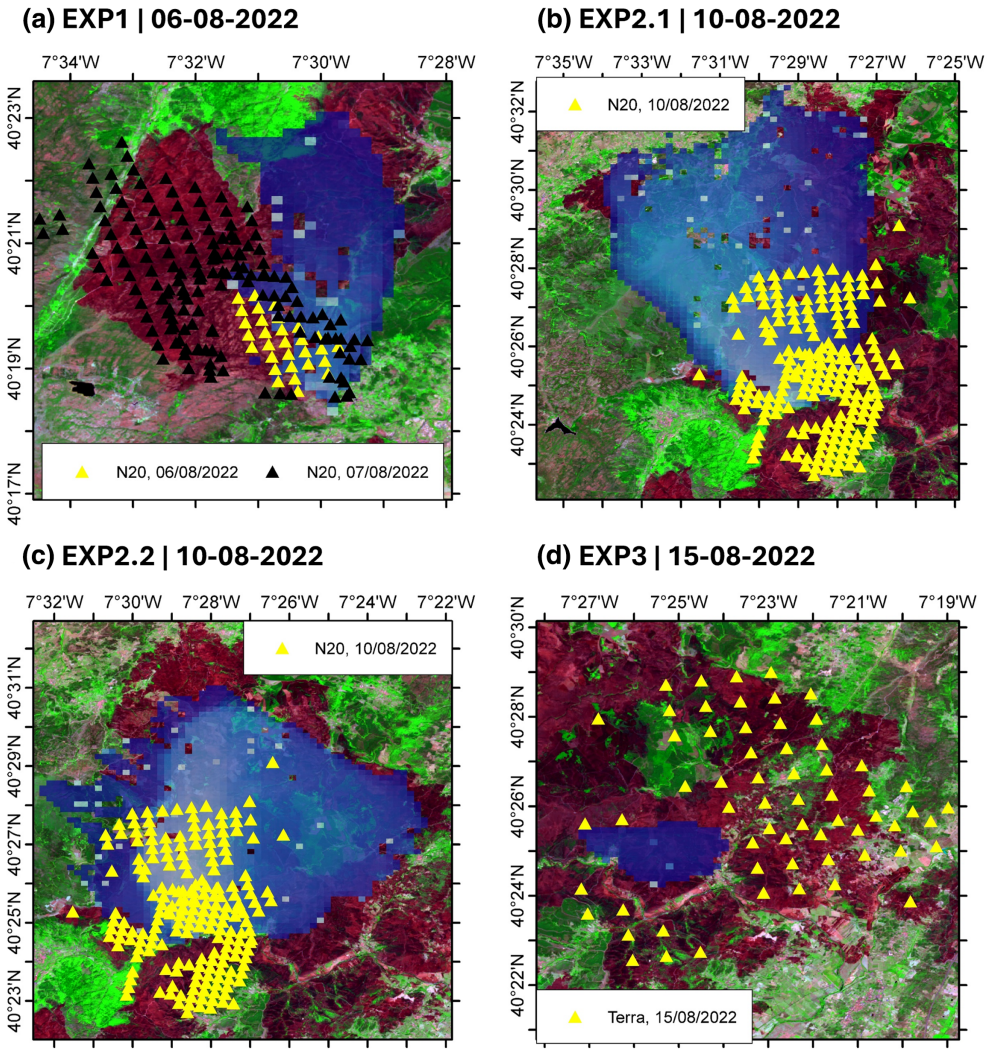

FIGURE 13 Comparison between the simulated fire spread (blue ramp color), active fire hotspots (triangles), and the RGB false-color composite derived from Sentinel-2 imagery for the following dates: (a) 6 August 2022 (EXP1 [IGN]); (b) 10 August 2022 (EXP2.1 [PYRO]); (c) 10 August 2022 (EXP2.2 [PYRO]); and (d) 15 August 2022 (EXP3 [REAC]). The colors of triangles in panel (a) represent different days. [Colour figure can be viewed at wileyonlinelibrary.com]

Vertical cross-sections of the simulations highlighted the fire's impact on the atmosphere, revealing strong updrafts and turbulent current flows originating from the fire. Among the three simulated periods, the most intense ascending currents were simulated on 10 August, coinciding with the development of pyro-convective clouds. Notably, in EXP2.2 [PYRO], these updrafts reached altitudes of up to 7000 meters and exhibited higher vertical velocities, along with strongest turbulence. In contrast, on the other days, updrafts peaked at altitudes between 3000 and 4000 meters with lower velocities and also weaker turbulence. Additionally, simulations performed for EXP2.2 without the ForeFire model (CTR) did not exhibit strong updrafts or turbulence, demonstrating that the presence of fire altered the atmosphere. Atmospheric turbulence plays a key role in both fire spread and smoke dispersion (e.g., Heilman, 2023). Fire, in turn, generates heat and intense vertical flows that produce additional turbulence. For instance, Clements et al. (2008) reported that fire-induced turbulence can reach five times the intensity of atmospheric turbulence. Efforts to better understand these processes have included numerical fire simulations (e.g., Mueller et al., 2014) as well as in situ measurements (e.g., Desai et al., 2023). In Portugal, the MesoNH/ForeFire modelling system has already been applied to understand pyro-convective events. Couto et al. (2024a) reported a vertical convective column reaching up to 10 km in the Pedrógão Grande fire, with turbulence values exceeding 10 $m^2 \cdot s^{-2}$ throughout the column. In Quiaios's fire, Campos et al. (2023) identified updrafts reaching middle levels, associated with smaller turbulence values of around 2 $m^2 \cdot s^{-2}$ at altitude; however, their simulations employed prescribed fire scenarios and did not incorporate dynamic fire spread. Conversely, Couto et al. (2024b) simulated updrafts extending up to 7 km using the full MesoNH/ForeFire coupled system, with turbulence values around 6 $m^2 \cdot s^{-2}$. Using the ACCESS-Fire model for wildfires in Australia, Peace et al. (2022) simulated pyro-convective cloud development up to 15 km in altitude with updrafts reaching

$32\,m{\cdot}s^{-1}$, while Peace et al. (2023) reported a cloud top reaching 12 km.

It is noteworthy that the EXP2.2 [PYRO] simulation, which exhibited stronger vertical velocities, also produced higher hydrometeor concentrations. Latent heat released during cloud microphysics processes further enhances the strength of the updrafts. This confirms that the presence of fire significantly modified the local atmosphere, facilitating the development of fire-induced convective clouds.

Both simulations for 10 August indicate a widespread burned area and the presence of multiple active-fire fronts. As documented by Mendonça et al. (2023), this scenario may have supplied additional energy to the environment, further accelerating the fire's growth and expansion. These combined factors likely enabled the fire to generate sufficient energy to sustain vertical development, ultimately leading to the observed pyro-convective activity. The simulations of 10 August indicated a strong fire–atmosphere coupling from the formation of pyro-convective clouds. Pyrocumulus (PyroCu) and pyrocumulonimbus (PyroCb) clouds have been associated with enhanced fire intensity and its dynamics can lead to changes in the fire front's propagation (e.g., Castellnou et al., 2022; Fromm et al., 2010; Rodriguez et al., 2020). In contrast, the two other simulated periods exhibited significantly lower smoke plume altitudes, suggesting that fire behavior on those days was primarily driven by wind and influenced by the complex topography, rather than by strong fire-induced convective processes. Beyond the complexity of fire–atmosphere interactions revealed in the studies mentioned above, the spread of fires is also influenced by mesoscale environmental conditions (Pinto et al., 2022b).

Concerning the fire propagation and total burned area, the visual comparison between the simulated burn area and observational data shows generally good agreement in the direction of fire spread across the analyzed dates, although some discrepancies are noted. On 6 August 2022, for instance, the model simulated northward fire progression, while the active-fire data showed a northwestward spread. However, the coarse spatial and temporal resolution of active-fire hotspot data limits the accuracy of comparisons between simulations and observations.

Finally, climate change is contributing to an increased frequency of droughts and an extended fire season (Pausas & Keeley, 2021). To mitigate the impacts of megafires, it is crucial to implement innovative monitoring and firefighting methodologies, as well as enhanced forest management strategies. Although megafires account for a small fraction of global wildfires, they have the most severe consequences for biodiversity (Duane et al., 2021; Tedim et al., 2020) and natural parks' attractiveness (Andrade et al., 2023). Beyond the immediate destructive effects, wildfires also lead to significant postfire impacts on affected regions, including soil erosion, changes in the hydrological regime, and increased risk of landslides. Following the wildfire in Serra da Estrela, rainfall in September and October of the same year triggered flooding events (Almeida et al., 2024). Landslides were also reported, resulting in road closures and adversely impacting local tourism (Almeida et al., 2024).

5 | LIMITATIONS AND CHALLENGES

Simulating a megafire is particularly challenging due to the complexity of the processes involved, the large spatial and temporal scales, and the substantial computational resources required. In this study, a coarser spatial resolution of 250 m was adopted compared to earlier 80-m simulations (Campos et al., 2023; Couto et al., 2024a, b). Despite this limitation, the model successfully reproduced pyro-convective cloud formation, showing that lower-resolution configurations can still provide valuable insights while remaining computationally feasible. Since the second simulated period favored cloud development, one of the challenges was identifying the meteorological clouds and those that would form from the fire's convective column. In this context, radar imagery with high temporal resolution enabled a more comprehensive assessment of the entire period during which clouds existed, making it possible to identify clouds originating from pyro-convection. High-resolution simulations further complemented the analysis by providing detailed insights that would otherwise remain undetected, helping to bridge gaps in observational data.

The present study also used a non-uniform fuel map in the ForeFire fire propagation model in addition to previous studies for Portugal, which allowed a more realistic representation of vegetation distribution and non-burnable areas, enhancing the credibility of fire behavior simulations. However, fuel is aggregated into simplified categories which does not capture the full structural and chemical diversity of real vegetation. Regarding the fire model, the ForeFire model does not account for firefighting actions, which may lead to simulated fire spread in areas where suppression was effective. Also, external factors that strongly influence fire dynamics, such as turbulence induced by firefighting aircraft (Mendonça et al., 2023) and the projection of firebrands capable of triggering secondary ignitions and merging fire fronts, are also not represented.

These limitations introduce uncertainty and highlight the need for continued model development. As emphasized by Coen (2018), many of these challenges are inherent to coupled fire–atmosphere systems, arising

for example from their numerical configuration and computational constraints. Nevertheless, coupled models remain powerful tools as they explicitly represent bidirectional fire–atmosphere interactions, allow the exploration of processes not directly observable in the field, and provide essential insights into wildfire dynamics.

6 | CONCLUSION

This study examined the 2022 wildfire in the Serra da Estrela Natural Park, a touristic destination and biodiversity hotspot in Portugal. Insights on fire behavior on three days were assessed from a fire–atmosphere coupled model approach, aiming to explore how changes in weather conditions can modify fire behavior in a medium term.

The synoptic analysis highlighted changes in large-scale atmospheric circulation over the study period, demonstrating that megafires developing over several days are vulnerable to these changes, which can directly influence the direction of fire front propagation. The study identified the development of low-pressure systems centered west of the Iberian Peninsula, which produced southerly and southwesterly winds over Portugal at 850 hPa. Furthermore, the approach of an upper-level trough associated with a cut-off low in the Bay of Biscay favored Northwesterly/Westerly winds in the study region. The impacts of these changes on the fire behavior were assessed by employing the MesoNH/ForeFire coupled system, which highlighted different scenarios during the event:

1. In the period encompassing fire ignition (EXP1 [IGN]), 6 August, the large-scale circulation brought warm, dry air from North Africa into the Iberian Peninsula, and a south/southeasterly flow was simulated near the surface. Such airflow influenced fire spread over the mountainous terrain, with the fire front spreading to north/northwest on 6 August, whereas the smoke plume remained within the lowest levels.
2. A similar fire-weather condition was identified in the second period (EXP2-[PYRO]), 10 August. However, the winds favored propagation of the fire front to the north/northwest in the morning of 10 August, and in different directions in the afternoon, initially to the north, then shifting to east, and later turning to west. Unlike the previous period [EXP1–IGN], the simulated periods on 10 August showed the convective plume reaching the middle levels and enabling the formation of pyro-convective clouds. In this context, the model successfully reproduced pyro-convective clouds, in good agreement with radar and satellite observations.
3. In the third period (EXP3–[REACT]), a strong north/northwesterly flow was seen on 15 August, leading to cooler and more humid weather conditions in the region. At the fire scale, the wind favored an eastward fire propagation, and the smoke plume was transported in the lower troposphere.

The simulations effectively captured key fire–atmosphere interactions, demonstrating the model's robustness and potential for operational forecasting. The regional meteorological conditions and local topographic features contributed to pyro-convection and fire spread on a smaller scale. However, this study highlights that megafire events, which last for several days or weeks, are directly affected by changes in weather conditions, which can either favor or hinder fire evolution.

Overall, the findings underscore the value of high-resolution coupled fire–atmosphere models for advancing the understanding of wildfire dynamics, as they explicitly simulate the two-way interactions between fire and atmosphere, thereby enabling more realistic forecasts of extreme events. Furthermore, their integration into operational platforms enhances decision-making for firefighting strategies and evacuation planning, reducing uncertainties and increasing the effectiveness of early warning protocols.

Given the ecological significance of natural parks, such as the Serra da Estrela region, improving the fire prediction capabilities is essential to support effective wildfire management and safeguard biodiversity, which have an important role for the recreational tourism activities developed in the park.

ACKNOWLEDGEMENTS

The authors are grateful to the European Centre for Medium-Range Weather Forecasts (ECMWF) for the meteorological analysis provided, the Portuguese Institute for Sea and Atmosphere (IPMA) for providing meteorological data and we acknowledge the data and/or imagery from NASA's Fire Information for Resource Management System (FIRMS) part of NASA's Land, Atmosphere Near real-time Capability for Earth observations (LANCE) and NASA's Earth Science Data and Information System (ESDIS). Open access publication funding provided by FCT (b-on).

FUNDING INFORMATION

The Portuguese Foundation for Science and Technology, I.P. (FCT) supported the work under the PyroC.pt. project (Refs. PCIF/MPG/0175/2019). This research was co-funded by the European Union through the European Regional Development Fund (FEDER) in the framework of the Interreg VI-A España-Portugal

(POCTEP) 2021–2027, FIREPOCTEP+ (0139_FIRE-POCTEP_MAS_6_E). The work is also funded by national funds through FCT in the framework of the UIDB/06107–Centro de Investigação em Ciência e Tecnologia para o Sistema Terra e Energia. Filippe L.M. Santos was supported by FCT by project reference 2022.11960.BD and DOI identifier https://doi.org/10.54499/2022.11960.BD, and Hugo Miguel Silva was supported by FCT Grant Number (2024.05649.BD).

DATA AVAILABILITY STATEMENT

The data that support the findings of this study are available from the corresponding author upon reasonable request.

ORCID

Cátia Campos https://orcid.org/0000-0002-1458-3732
Filippe L. M. Santos https://orcid.org/0000-0001-8680-1244
João Rio https://orcid.org/0000-0003-4457-4543
Manuel Lopes https://orcid.org/0000-0002-7116-9802

REFERENCES

Almeida, M., Soviev, M., San-Miguel, J., Durrant, T., Oom, D., Branco, A. et al. (2024) *Report on the large wildfires of 2022 in Europe*. Luxembourg: Publications Office of the European Union.

Andrade, N., Couto, F.T. & Serra, J. (2023) Assessing fire risk perception in the Vale do Guadiana Natural Park, Portugal. *Fire*, 6(6), 243. Available from: https://doi.org/10.3390/fire6060243

Bento-Gonçalves, A. (2021) *Os Incêndios Florestais Em Portugal*, Vol. 108. Lisbon: Fundação Francisco Manuel Dos Santos, p. 112.

Calheiros, T., Pereira, M.G. & Nunes, J.P. (2021) Assessing impacts of future climate change on extreme fire weather and pyro-regions in Iberian Peninsula. *Science of the Total Environment*, 754(2021), 142233. Available from: https://doi.org/10.1016/j.scitotenv.2020.142233

Campos, C., Couto, F.T., Filippi, J.-B., Baggio, R. & Salgado, R. (2023) Modelling pyro-convection phenomenon during a mega-fire event in Portugal. *Atmospheric Research*, 290(2023), 106776. Available from: https://doi.org/10.1016/j.atmosres.2023.106776

Carmo, M., Ferreira, J., Mendes, M., Silva, Á., Silva, P., Alves, D. et al. (2021) The climatology of extreme wildfires in Portugal, 1980–2018: contributions to forecasting and preparedness. *International Journal of Climatology*, 42(5), 3123–3146. Available from: https://doi.org/10.1002/joc.7411

Castellnou, M., Bachfischer, M., Miralles, M., Ruiz, B., Stoof, C.R. & Vilà-Guerau de Arellano, J. (2022) Pyroconvection classification based on atmospheric vertical profiling correlation with extreme fire spread observations. *Journal of Geophysical Research: Atmospheres*, 127(22), 26. Available from: https://doi.org/10.1029/2022jd036920

Cheung, K., Sharples, J., Favero, D.D. & Cortes, C.T. (2025) Dynamic fire-atmosphere interaction in the 2020 Montana Bridger foothills wildfire as revealed by WRF-SFIRE simulations. *Npj Natural Hazards.*, 2(1), 10. Available from: https://doi.org/10.1038/s44304-025-00132-0

Clements, C.B., Zhong, S., Bian, X., Heilman, W.E. & Byun, D.W. (2008) First observations of turbulence generated by grass fires. *Journal of Geophysical Research*, 113(D22), 13. Available from: https://doi.org/10.1029/2008jd010014

Clough, K., Farguell, A., Mandel, J., Hilburn, K. & Kochanski, A. (2025) Enhancing wildfire and smoke forecasting by integrating fire observations: a comparative analysis of methods for integrating infrared and satellite data into a coupled fire-atmosphere model. *Journal of Geophysical Research: Atmospheres*, 130(12), 19. Available from: https://doi.org/10.1029/2024jd042561

Coen, J. (2018) Some requirements for simulating wildland fire behavior using insight from coupled weather—wildland fire models. *Fire*, 1(1), 6. Available from: https://doi.org/10.3390/fire1010006

Countryman, C.M. (1972) *The fire environment concept*. California: Pacific Southwest Forest and Range Experiment Station.

Couto, F.T., Campos, C., Purificação, C., Santos, M., Andrade, H.N., Andrade, N. et al. (2025b) Synoptic and regional meteorological drivers of a wildfire in the wildland–urban Interface of Faro (Portugal). *Fire*, 8(9), 362. Available from: https://doi.org/10.3390/fire8090362

Couto, F.T., Filippi, J.-B., Baggio, R., Campos, C. & Salgado, R. (2024a) Numerical investigation of the Pedrógão Grande pyrocumulonimbus using a fire to atmosphere coupled model. *Atmospheric Research*, 299, 107223. Available from: https://doi.org/10.1016/j.atmosres.2024.107223

Couto, F.T., Filippi, J.-B., Baggio, R., Campos, C. & Salgado, R. (2024b) Triggering pyro-convection in a high-resolution coupled fire–atmosphere simulation. *Fire*, 7(3), 92. Available from: https://doi.org/10.3390/fire7030092

Couto, F.T., Santos, F.L.M., Campos, C., Andrade, N., Purificação, C. & Salgado, R. (2022) Is Portugal starting to burn all year long? The transboundary fire in January 2022. *Atmosphere*, 13(10), 1677. Available from: https://doi.org/10.3390/atmos13101677

Couto, F.T., Santos, F.L.M., Campos, C., Purificação, C., Andrade, N., López-Veja, J.M. et al. (2024c) A case study of the possible meteorological causes of unexpected fire behavior in the Pantanal wetland, Brazil. *Earth*, 5, 548–563. Available from: https://doi.org/10.3390/earth5030028

Couto, F.T., Santos, F.L.M., Campos, C., Purificação, C., Andrade, N., Lopez-Veja, J.M. et al. (2025a) Exploratory analysis of atmospheric modelling use over Pantanal wildfires. *RAEGA-O Espaço Geográfico Em Análise*, 63(2), 35–56. Available from: https://doi.org/10.5380/raega.v63i2.99955

Cuxart, J., Bougeault, P. & Redelsperger, J.-L. (2000) A turbulence scheme allowing for mesoscale and large-eddy simulations. *Quarterly Journal of the Royal Meteorological Society*, 126(562), 1–30. Available from: https://doi.org/10.1002/qj.49712656202

de la Barrera, F., Barraza, F., Favier, P., Ruiz, V. & Quense, J. (2018) Megafires in Chile 2017: monitoring multiscale environmental impacts of burned ecosystems. *Science of the Total Environment*, 637, 1526–1536. Available from: https://doi.org/10.1016/j.scitotenv.2018.05.119

Desai, A., Heilman, W.E., Skowronski, N.S., Clark, K.L., Gallagher, M.R., Clements, C.B. et al. (2023) Features of turbulence during wildland fires in forested and grassland environments. *Agricultural and Forest Meteorology*, 338, 109501. Available from: https://doi.org/10.1016/j.agrformet.2023.109501

Di Virgilio, G., Evans, J.P., Blake, S.A.P., Armstrong, M., Dowdy, A.J., Sharples, J. et al. (2019) Climate change increases the potential for extreme wildfires. *Geophysical Research Letters*, 46(14), 8517–8526. Available from: https://doi.org/10.1029/2019gl083699

Dickman, C.R. (2021) Ecological consequences of Australia's "black summer" bushfires: managing for recovery. *Integrated Environmental Assessment and Management*, 17(6), 1162–1167. Available from: https://doi.org/10.1002/ieam.4496

Duane, A., Castellnou, M. & Brotons, L. (2021) Towards a comprehensive look at global drivers of novel extreme wildfire events. *Climatic Change*, 165(3–4), 43. Available from: https://doi.org/10.1007/s10584-021-03066-4

Evans, D. (2012) Building the European Union's Natura 2000 network. *Nature Conservation*, 1(11–26), 11–26. Available from: https://doi.org/10.3897/natureconservation.1.1808

Filippi, J.-B., Bosseur, F., Mari, C. & Lac, C. (2018) Simulation of a large wildfire in a coupled fire-atmosphere model. *Atmosphere*, 9(6), 218. Available from: https://doi.org/10.3390/atmos9060218

Filippi, J.B., Bosseur, F., Mari, C., Lac, C., Le Moigne, P., Cuenot, B. et al. (2009) Coupled atmosphere–wildland fire modelling. *Journal of Advances in Modeling Earth Systems*, 1(4), 9. Available from: https://doi.org/10.3894/james.2009.1.11

fogos.pt. (2022) Report. Fogos.pt. Available at: https://fogos.pt/ [Accessed 12th May 2025].

Fromm, M., Lindsey, D.T., Servranckx, R., Yue, G., Trickl, T., Sica, R. et al. (2010) The untold story of Pyrocumulonimbus. *Bulletin of the American Meteorological Society*, 91(9), 1193–1210. Available from: https://doi.org/10.1175/2010BAMS3004.1

Gouveia, C.M., Bastos, A., Trigo, R.M. & DaCamara, C.C. (2012) Drought impacts on vegetation in the pre- and post-fire events over Iberian Peninsula. *Natural Hazards and Earth System Sciences*, 12(10), 3123–3137. Available from: https://doi.org/10.5194/nhess-12-3123-2012

Güngöroğlu, C. (2018) Forest Fire Studies on Fire Behaviour: Key Topics and Their Importance. In: *14th International Combustion Symposium (INCOS2018)*, 25–27 April 2018, Faculty of Forestry, Demir-Çelik Kampüsü, Karabük, Turkey.

Hegedűs, D., Ballinger, A.P. & Hegerl, G.C. (2024) Observed links between heatwaves and wildfires across northern high latitudes. *Environmental Research Letters*, 19(3), 034041–034041. Available from: https://doi.org/10.1088/1748-9326/ad2b29

Heilman, W.E. (2023) Atmospheric turbulence and wildland fires: a review. *International Journal of Wildland Fire*, 32, 476–495. Available from: https://doi.org/10.1071/wf22053

ICNF. (2025) Territórios ardidos. Icnf.pt. Available at: https://sig.icnf.pt/portal/home/item.html?id=983c4e6c4d5b4666b258a3ad5f3ea5af [Accessed 1st September 2025].

IPMA. (2022) Incêndios Rurais. Análise meteorológica & Índices de perigo e de risco. In IPMA. Available at: https://www.ipma.pt/pt/index.html [Accessed 12th May 2025].

Jansen, J. (2011) Managing Natura 2000 in a changing world: the case of the Serra da Estrela (Portugal). *BMC Public Health*. Radboud University Nijmegen. https://repository.ubn.ru.nl/bitstream/handle/2066/90921/90921.pdf?sequence=1&isAllowed=y

Kartsios, S., Karacostas, T., Pytharoulis, I. & Dimitrakopoulos, A.P. (2021) Numerical investigation of atmosphere-fire interactions during high-impact wildland fire events in Greece. *Atmospheric Research*, 247(2021), 105253. Available from: https://doi.org/10.1016/j.atmosres.2020.105253

Lac, C., Chaboureau, J.-P., Masson, V., Pinty, J.-P., Tulet, P., Escobar, J. et al. (2018) Overview of the meso-NH model version 5.4 and its applications. *Geoscientific Model Development*, 11(5), 1929–1969. Available from: https://doi.org/10.5194/gmd-11-1929-2018

Lareau, N.P. & Clements, C.B. (2017) The mean and turbulent properties of a wildfire convective plume. *Journal of Applied Meteorology and Climatology*, 56(8), 2289–2299. Available from: https://doi.org/10.1175/jamc-d-16-0384.1

Lareau, N.P., Nauslar, N.J. & Abatzoglou, J.T. (2018) The Carr fire vortex: a case of Pyrotornadogenesis? *Geophysical Research Letters*, 45(23), 13,107–13,115. Available from: https://doi.org/10.1029/2018gl080667

Libonati, R., Geirinhas, J.L., Silva, P.S., Russo, A., Rodrigues, J.A., Belém, L.B.C. et al. (2022) Assessing the role of compound drought and heatwave events on unprecedented 2020 wildfires in the Pantanal. *Environmental Research Letters*, 17(1), 015005. Available from: https://doi.org/10.1088/1748-9326/ac462e

Linley, G.D., Jolly, C.J., Doherty, T.S., Geary, W.L., Armenteras, D., Belcher, C.M. et al. (2022) What do you mean, "megafire"? *Global Ecology and Biogeography*, 31(10), 1906–1922. Available from: https://doi.org/10.1111/geb.13499

Lusa. (2022) Incêndio de agosto foi o maior em 47 anos na serra. ECO; Eco. Available at: https://eco.sapo.pt/2022/12/26/incendio-de-agosto-foi-o-maior-em-47-anos-na-serra-da-estrela/ [Accessed 12th May 2025].

Malinowski, R., Lewiński, S., Rybicki, M., Gromny, E., Jenerowicz, M., Krupiński, M. et al. (2020) Automated production of a land cover/use map of Europe based on Sentinel-2 imagery. *Remote Sensing*, 12(21), 3523. Available from: https://doi.org/10.3390/rs12213523

Mario, E., Raffaele, L., Onofrio, C., Josè Maria, C.-S., Valentina, B., Vincenzo, G. et al. (2024) Coupling heat wave and wildfire occurrence across multiple ecoregions within a Eurasia longitudinal gradient. *The Science of the Total Environment*, 912, 169269. Available from: https://doi.org/10.1016/j.scitotenv.2023.169269

Masson, V., Le Moigne, P., Martin, E., Faroux, S., Alias, A., Alkama, R. et al. (2013) The SURFEXv7.2 land and ocean surface platform for coupled or offline simulation of earth surface variables and fluxes. *Geoscientific Model Development*, 6(4), 929–960. Available from: https://doi.org/10.5194/gmd-6-929-2013

Mayers, L. (2024) Fuelling Mega Fires-International Association of Wildland Fire. International Association of Wildland Fire. Available at: https://www.iawfonline.org/article/fuelling-mega-fires/ [Accessed 12th May 2025].

Mendonça, J.M., Mágoas, C., Pereira, J.M.C., Fernandes, P., Viegas, D.X., Tedim, F. et al. (2023) Relatório final do grupo de peritos dos incêndios rurais. In AGIF. Available at: https://www.agif.pt/app/uploads/2023/04/Relat%C3%B3rio-Final-do-Grupo-de-Peritos-dos-Inc%C3%AAndios-Rurais.pdf.

Mlawer, E.J., Taubman, S.J., Brown, P.D., Iacono, M.J. & Clough, S.A. (1997) Radiative transfer for inhomogeneous atmospheres: RRTM, a validated correlated-k model for the longwave. *Journal of Geophysical Research: Atmospheres*, 102(D14), 16663–16682. Available from: https://doi.org/10.1029/97jd00237

Moreira, F., Catry, F.X., Rego, F. & Bacao, F. (2010) Size-dependent pattern of wildfire ignitions in Portugal: when do ignitions turn into big fires? *Landscape Ecology*, 25, 1405–1417. Available from: https://doi.org/10.1007/s10980-010-9491-0

Mueller, E., Mell, W. & Simeoni, A. (2014) Large eddy simulation of forest canopy flow for wildland fire modeling. *Canadian Journal of Forest Research*, 44(12), 1534–1544. Available from: https://doi.org/10.1139/cjfr-2014-0184

Nojarov, P. & Nikolova, M. (2022) Heat waves and forest fires in Bulgaria. *Natural Hazards*, 114, 1879–1899. Available from: https://doi.org/10.1007/s11069-022-05451-3

Nunes, L.J.R., Raposo, M.A.M., Meireles, C.I.R., Gomes, C.J.P. & Ribeiro, N.M.C.A. (2021) Energy recovery of shrub species as a path to reduce the risk of occurrence of rural fires: a case study in Serra da Estrela Natural Park (Portugal). *Fire*, 4(3), 33. Available from: https://doi.org/10.3390/fire4030033

Parente, J., Amraoui, M., Menezes, I. & Pereira, M.G. (2019) Drought in Portugal: current regime, comparison of indices and impacts on extreme wildfires. *Science of the Total Environment*, 685, 150–173. Available from: https://doi.org/10.1016/j.scitotenv.2019.05.298

Pausas, J.G. & Keeley, J.E. (2021) Wildfires and global change. *Frontiers in Ecology and the Environment*, 19(7), 387–395.

Peace, M., Greenslade, J., Ye, H. & Kepert, J.D. (2022) Simulations of the Waroona fire using the coupled atmosphere–fire model ACCESS-fire. *Journal of Southern Hemisphere Earth Systems Science*, 72(2), 126–138. Available from: https://doi.org/10.1071/es22013

Peace, M., Ye, H., Greenslade, J. & Kepert, J.D. (2023) The destructive sir Ivan fire in New South Wales, Australia; simulations using a coupled fire—atmosphere model. *Fire*, 6(11), 438–438. Available from: https://doi.org/10.3390/fire6110438

Peterson, D.A., Campbell, J.R., Hyer, E.J., Fromm, M.D., Kablick, G.P., Cossuth, J.H. et al. (2018) Wildfire-driven thunderstorms cause a volcano-like stratospheric injection of smoke. *npj Climate and Atmospheric Science*, 1(1), 8. Available from: https://doi.org/10.1038/s41612-018-0039-3

Peterson, D.A., Fromm, M.D., McRae, R.H.D., Campbell, J.R., Hyer, E.J., Taha, G. et al. (2021) Australia's black summer pyrocumulonimbus super outbreak reveals potential for increasingly extreme stratospheric smoke events. *npj Climate and Atmospheric Science*, 4(1), 38. Available from: https://doi.org/10.1038/s41612-021-00192-9

Pinto, P., Silva, Á., Viegas, D., Almeida, M. & Ribeiro, L. (2022a) Influence of a sea-breeze front over a fire plume, Pedrogão Grande wildfires. uc.pt. https://books.uc.pt/chapter?chapter=978989262298942

Pinto, P., Silva, Á.P., Viegas, D.X., Almeida, M., Raposo, J. & Ribeiro, L.M. (2022b) Influence of convectively driven flows in the course of a large fire in Portugal: the case of Pedrógão Grande. *Atmosphere*, 13(3), 414. Available from: https://doi.org/10.3390/atmos13030414

Pinty, J.-P. & Jabouille, P. (1998) A mixed-phase cloud parameterization for use in a mesoscale non-hydrostatic model: simulations of a squall line and of orographic precipitation. Bulletin of the American Meteorological Society Proceedings of the Conference of Cloud Physics, Everett, WA, USA.

Prabhakaran, A. & Srivastava, P. (2025) Analysis of prevailing atmospheric conditions during wildfire events in the Indian Himalayan region. *Quarterly Journal of the Royal Meteorological Society*, 151(767), e4918. Available from: https://doi.org/10.1002/qj.4918

Purificação, C., Campos, C., Henkes, A. & Couto, F.T. (2024) Exploring the atmospheric conditions increasing fire danger in the Iberian Peninsula. *Quarterly Journal of the Royal Meteorological Society*, 150(763), 3475–3494. Available from: https://doi.org/10.1002/qj.4776

Purificação, C., Santos, F.L., Henkes, A., Kartsios, S. & Couto, F.T. (2025) Fire-weather conditions during two fires in southern Portugal: meteorology, orography, and fuel characteristics. *Modeling Earth Systems and Environment*, 11(2), 17. Available from: https://doi.org/10.1007/s40808-025-02308-z

Redelsperger, J.L. & Sommeria, G. (1981) Methode de representation de la turbulence d'echelle inferieure a la maille pour un modele tri-dimensionnel de convection nuageuse. *Boundary-Layer Meteorology*, 21(4), 509–530. Available from: https://doi.org/10.1007/bf02033598

Rodrigues, M., Trigo, R.M., Vega-García, C. & Cardil, A. (2020) Identifying large fire weather typologies in the Iberian Peninsula. *Agricultural and Forest Meteorology*, 280, 107789. Available from: https://doi.org/10.1016/j.agrformet.2019.107789

Rodriguez, B., Lareau, N.P., Kingsmill, D.E. & Clements, C.B. (2020) Extreme Pyroconvective updrafts during a megafire. *Geophysical Research Letters*, 47(18), 9. Available from: https://doi.org/10.1029/2020gl089001

Ruffault, J., Curt, T., Moron, V., Trigo, R.M., Mouillot, F., Koutsias, N. et al. (2020) Increased likelihood of heat-induced large wildfires in the Mediterranean Basin. *Scientific Reports*, 10(1), 13790. Available from: https://doi.org/10.1038/s41598-020-70069-z

San-Miguel-Ayanz, J., Oom, D., Artès, T., Viegas, D.X., Fernandes, P., Faivre, N. et al. (2020) *Super case study: Forest fires in Portugal in 2017*. Luxembourg: Publications Office of the European Union.

Silva, V., Catry, F.X., Fernandes, P., Rego, F.C., Paes, P., Nunes, L. et al. (2019) Effects of grazing on plant composition, conservation status and ecosystem services of Natura 2000 shrub-grassland habitat types. *Biodiversity and Conservation*, 28, 1205–1224. Available from: https://doi.org/10.1007/s10531-019-01718-7

Sullivan, A.L. (2017) Inside the inferno: fundamental processes of wildland fire behaviour. Part I: combustion Chemestry and heat release. *Current Forestry Reports*, 3(2), 132–149. Available from: https://doi.org/10.1007/s40725-017-0057-0

Tedim, F., Leone, V., Coughlan, M.R., Bouillon, C., Xanthopoulos, G., Royé, D. et al. (2020) Extreme wildfire events: the definition. In: *Extreme wildfire events and disasters: root causes and new management strategies*. Netherlands: Elsevier, pp. 3–29.

Toivanen, J., Engel, C.B., Reeder, M.J., Lane, T.P., Davies, L., Webster, S. et al. (2019) Coupled atmosphere-fire simulations of the black Saturday Kilmore east wildfires with the unified model. *Journal of Advances in Modeling Earth Systems*, 11(1), 210–230. Available from: https://doi.org/10.1029/2017ms001245

Trigo, R.M., Pereira, J.M.C., Pereira, M.G., Mota, B., Calado, T.J. & DaCamara, C.C. (2006) Atmospheric conditions associated with

the exceptional fire season of 2003 in Portugal. *International Journal of Climatology*, 26, 1741–1757. Available from: https://doi.org/10.1002/joc.1333

Turco, M., Jerez, S., Augusto, S., Tarín-Carrasco, P., Ratola, N., Jiménez-Guerrero, P. et al. (2019) Climate drivers of the 2017 devastating fires in Portugal. *Scientific Reports*, 9(1), 13886. Available from: https://doi.org/10.1038/s41598-019-50281-2

Vaz, R., Silva, R., Cardoso Pereira, S., Carvalho, A.C., Carvalho, D. & Rocha, A. (2025) Coupled atmosphere–fire modelling of Pyro-convective activity in Portugal. *Fire*, 8(4), 153. Available from: https://doi.org/10.3390/fire8040153

Wagner, V. (1987) Development and structure of the Canadian Forest Fire Weather Index System.

Zoom Earth. (2025) Zoom Earth. Available at: https://zoom.earth/ [Accessed 12th May 2025].

SUPPORTING INFORMATION

Additional supporting information can be found online in the Supporting Information section at the end of this article.

How to cite this article: Campos, C., Couto, F.T., Santos, F.L.M., Pinto, P., Purificação, C., Silva, H.M. *et al*. (2026) Assessing wildfire dynamics during a megafire in Portugal using the MesoNH/ForeFire coupled model. *Quarterly Journal of the Royal Meteorological Society*, 152:e70075. Available from: https://doi.org/10.1002/qj.70075